Hydrological Processes

WILEY

RESEARCH ARTICLE OPEN ACCESS

Advancing Hydrologic Modelling Through Bias Correcting Weather Radar Data: The Valgrosina Case Study in the Italian Alps

Andrea Citrini[1] | Georgia Lazoglou[2] | Adriana Bruggeman[3] | George Zittis[2] | Giovanni P. Beretta[1] | Corrado A. S. Camera[1]

[1]Dipartimento di Scienze Della Terra "Ardito Desio", Università Degli Studi di Milano, Milan, Italy | [2]Climate and Atmosphere Research Center (CARE-C), The Cyprus Institute, Nicosia, Cyprus | [3]Energy, Environment and Water Research Center (EEWRC), The Cyprus Institute, Nicosia, Cyprus

Correspondence: Andrea Citrini (andrea.citrini@unimi.it)

Received: 21 May 2024 | **Revised:** 17 September 2024 | **Accepted:** 3 November 2024

Funding: This work was supported by Italian Ministry of Education, University and Research (MIUR).

Keywords: GEOframe model | northern Italy | radar correction | statistical corrections | water management | water resources

ABSTRACT

The urgency of understanding the intricate input–output relationships of the hydrologic cycle is amplified by the accelerating climate change impacts in mountain environments. This study focuses on optimising water resource management of a dammed valley in the Central Alps (Northern Italy). The research aims to integrate radar data and precipitation interpolation techniques (TIN, Copula, cumulative distribution function; CDF techniques, inverse distance weighting; IDW, thin plate spline; TPS, ordinary kriging; OK and detrended kriging; DK) into a semi-distributed hydrologic model, by utilising hourly precipitation data from 22 rain gauges and a composite weather radar product spanning 2010–2020. Two main objectives were pursued: (i) to develop and evaluate various radar precipitation correction methods against a benchmark dataset and (ii) to calibrate and assess the performance of the GEOFrame hydrologic model forced with corrected precipitation input. Point-based and spatial correction approaches were evaluated against ground measurements through leave-one-out tests. The former derives dependence functions between the biased radar series and those of the closest three rain gauges to the target point applying a triangular irregular network. The latter combines deterministic and geospatial interpolations to the rain gauge/radar residuals to derive a corrected surface by incorporating radar values as trends. Precipitation series exceeding the composite scaled score of the benchmark dataset were used as input for hydrologic modelling. The spatial method combining radar values with ordinary kriging provided the best results for both correction and modelling (hourly KGE > 0.75). The spatial approaches proved easier to apply than the point-based methods. In addition, correcting precipitation significantly improved low-flow simulation from negative hourly lnNSE to values greater than 0.25. As a further step, given the overall good performance of the spatial methods, they could be used operationally as an ensemble to analyse management scenarios.

1 | Introduction

Hydrologic models are an essential tool to model the water cycle of a given area for water resource management (Devia, Ganasri, and Dwarakish 2015). Over the past decades, the variety and complexity of hydrologic models have increased exponentially in response to the need to solve problems at different scales and of different nature (Ly, Charles, and Degré 2013). The most common applications include forecasts and predictions for climate impact studies (Asong et al. 2020; Cochand, Therrien, and Lemieux 2019; Cornelissen, Diekkrüger, and Giertz 2013; Hegerl et al. 2015;

Karlsson et al. 2016), optimised water resource management (Madrazo-Uribeetxebarria et al. 2021; Paul et al. 2021; Qin et al. 2013), flood hazard governance and early warning (Charlton et al. 2006; Mudashiru et al. 2021; Norman et al. 2010; Sampson et al. 2015), and land use changes assessments (Jordan, Ghulam, and Hartling 2014; Wegehenkel 2002; Yan et al. 2013; Zhang et al. 2020).

Among other factors, the choice of hydrologic model complexity level is driven by the availability and quality of the forcing data, which are often scattered in space and time. Among the input data, precipitation is the most essential because it regulates the amount of water entering the system and, thus, it is deeply connected to all other environmental processes as a trigger, although not in a linear way (Berne and Krajewski 2013). By excluding lumped models, where a point series of a rain gauge is sufficient, all distributed models (semi and fully) need spatialized rainfall information at the most accurate level possible to represent the spatial and temporal variability of the phenomenon (Bell and Moore 2000; Segond, Wheater, and Onof 2007). Thiessen polygons, inverse distance weighting (IDW), linear regression and ordinary kriging (OK) are common techniques for interpolating data from weather stations scattered around the study area to obtain a continuous field to feed the model at the required locations (Caruso and Quarta 1998; Mair and Fares 2011). The application of such methods becomes increasingly complex when the area of interest is characterised by complex topography, steep mountains or the proximity of large water bodies (Buytaert et al. 2006; Camera et al. 2014; Johnson and Hanson 1995). In mountainous areas, the orographic and rain shadow effects can contribute significantly to local variation in precipitation. The former favours increasing precipitation based on increasing elevation (Groisman and Easterling 1994; Sevruk 1997; Sinclair et al. 1997; Weisse and Bois 2001), while the latter describes the phenomenon whereby mountains hinder the movement of moist air masses, causing precipitation to occur predominantly on the windward side areas (Stockham et al. 2018; Van Den Hende et al. 2021).

The need to acquire data with spatial and temporal continuity was partially solved with the development of weather radar technology in the years following World War II (Atlas 1964; Rogers and Smith 1996). Nevertheless, the high spatio-temporal resolution data provided by radars have not gained overwhelming popularity as input data for hydrologic models (Berne and Krajewski 2013). Weather radars do not directly measure the amount of rainfall but are based on measurements of the electromagnetic properties of hydrometeors, including rain, snow and hail. These measurements can be converted to rainfall rates and then validated against observations from weather stations (Berne and Krajewski 2013; Ochoa-Rodriguez et al. 2019). Several factors, such as, for example, signal attenuation due to severe precipitation, beam obstruction and ground clutter due to morphological or structural limitations, reduce the accuracy of the radar measurements, resulting in biased values compared with the observed ones and making them unsuitable as direct input in hydrologic models (Bárdossy and Pegram 2017; Biggs and Atkinson 2011; Kim, Kwon, and Lima 2018; Seo 1998; Seo, Breidenbach, and Johnson 1999). However, calibration and validation of these data can be complex and time-consuming. Moreover, integrating radar data into hydrologic models requires additional pre-processing steps. This complexity can discourage modellers from using radar data, especially if they have well-established working methodologies that use other data sources such as rain gauge networks and satellite products.

An overview of the main correction techniques and their classification is presented in Ochoa-Rodriguez et al. (2019). These are distinguished into geostatistical and non-geostatistical methods or, depending on the application, adjustment or integration methods. The combination of the classification of Wang et al. (2013) and Decloedt, Willems, and Gires (2013) is interesting since it is based on the purpose of the application. This classification divides approaches into methods that focus on bias-correcting the radar data (attempting to correct the bias present in radar accumulations using rain gauge accumulations as the true rainfall value); rain gauge interpolation methods using radar spatial association as additional information, which exploit the radar field to aid the spatial interpolation of point rain gauge values; and radar and rain gauge integration methods (in this case, rainfall at a given location is estimated through a weighted average between the radar and rain gauge values). The main techniques used for correction and combination of radar and rain gauge data are called bias correction (Mapiam et al. 2022; Rabiei and Haberlandt 2015; Seo and Breidenbach 2002). Common bias correction approaches include linear scaling, mean-field bias correction, and quantile mapping, while spatial interpolation methods are commonly used for filling gaps between radar pixels (Foehn et al. 2018; Haberlandt 2007; Teegavarapu, Meskele, and Pathak 2012). Kriging, IDW and spline interpolation are applied to obtain continuous precipitation fields. Additionally, temporal smoothing techniques (Berndt, Rabiei, and Haberlandt 2014; Villarini et al. 2014; Wright et al. 2014) have been used to obtain, through moving averages or filtering methods, more stable and realistic precipitation values. Hydrometeor classification (Gao and Stensrud 2012; Snyder et al. 2010) and dual polarisation correction (Anagnostou et al. 2010; Gorgucci and Chandrasekar 2005; Shakti et al. 2013) are additional methods, where the echoes of various types of hydrometeors are classified through algorithms improving the accuracy of precipitation estimates, particularly for mixed-phase precipitation. In recent years, the Copula method based on the Sklar theorem (Sklar 1959) has begun to be used frequently to describe the complex spatio-temporal relationship between radar and weather station data, which is much more complex than the assumption of linear behaviour (Bárdossy 2006; Bárdossy and Li 2008; Gómez-Hernández and Wen 1998). Examples of correction of radar data by copula can be found in Hamidi, Farnham, and Khanbilvardi (2018), Mao et al. (2015) and Vogl et al. (2012). An estimation of error and uncertainty ranges by the same method is reported in AghaKouchak, Bárdossy, and Habib (2010), Dai et al. (2016, 2014) and Villarini et al. (2014). The use of copula is also widely applied for the correction of data from climate models, for example, Alidoost et al. (2017), Lazoglou et al. (2022, 2020) and Maity et al. (2019).

This study aims to integrate radar data and precipitation interpolation into a semi-distributed hydrologic model by combining hourly rain gauge network data and weather radar.

As specific objectives, (i) different radar precipitation correction methods were developed and assessed against a benchmark dataset, (ii) the semi-distributed hydrological model forced with corrected precipitation inputs was calibrated for each parameter configuration and (iii) its performances of were evaluated. By directly incorporating radar signals, valuable information is retained without sacrificing accuracy. The underlying assumption is that rain gauge measurements are accurate, and radar data offer supplementary insights (Haberlandt 2007). Improving the understanding of the intricate input–output relationships of the hydrological cycle plays a key role in optimising water resource management. This is particularly relevant in a context such as Italy, where, in 2022, the annual rainfall amounted to just 50% of the 1991–2020 climatological average (Braca et al. 2023), impacting the hydroelectric production of Alpine power plants with losses of −37% compared with the previous year (Terna 2022). Focused on a pilot area within the Italian Alps bordering Switzerland, this research is particularly well-suited to address this challenge due to the area's complex terrain, dense rainfall network, availability of weather radar data and hydropower exploitation.

2 | Data and Methods

2.1 | Study Area

The study area is in Valgrosina, a tributary valley of Valtellina Valley. The valley has an area of about 130 km^2, and is located in northern Italy partially bordering Switzerland (Figure 1). This is divided into three main sectors: the downstream part covering the territory of the village of Grosio (from which the valley takes its name, approximately 650–1200 m a.s.l.), and the upper section divided into two parts by the Roasco Stream, the Eita Valley (N–S, 1200–3370 m a.s.l.) and the Sacco Valley (W–E, 1200–3260 m a.s.l.), respectively. Valgrosina belongs to the sector of the Upper Valtellina between the small mountain cities of Tirano and Bormio, which is geologically characterised by schistose and intrusive rocks (Notarpietro 1988), distinguished within the Upper Austroalpine domain according to their structural characteristics (Beltrami et al. 1971; Bonsignore et al. 1969; Pozzi, Bollettinari, and Clerici 1990). More specifically, in Valgrosina, the predominant lithologies are gneisses and micaschists of the Lower Cambrian and the Upper Ordovician (Gregnanin and Montrasio 1990). In addition to being subject to glacial and periglacial morphogenesis, this area has been strongly influenced by tectonic activity (Forcella 1984; Fossati and Mannucci 1996; Pozzi, Bollettinari, and Clerici 1990). The main tectonic lineaments are the "Linea Insubrica" and "Linea del Mortirolo" faults, but there are also minor dislocation systems, dense and numerous with prevailing NW–SE, NE–SW and N–S directions that profoundly influenced the development of the hydrographic network (Assi et al. 1995).

The climate is of central-alpine type (Belloni and Pelfini 1987), with medium-low average annual precipitation (800–1000 mm at the medium altitudes between 1000 and 1500 m a.s.l.), which in extremely wet years can reach values around 1700 $mm y^{-1}$ (Ceriani and Carelli 2000). The rainiest season is spring–summer. The average annual temperature value is around 20°C in the medium part of the valley and decreases going further inland and at higher altitudes (Assi et al. 1995).

Since the 20th century, dams and hydroelectric plants have been built in Italy to regulate the flow of natural watercourses, creating a water reserve for periods of drought, and exploiting the resource for the generation of clean energy (Bocchiola and Rosso 2014; McCully 2001; World Commission on Dams 2000). In the case of the Upper Valtellina, there was intense interest beginning in the early decades of the 1900s to provide electricity for the tramways and lighting of the city of Milan (Toso 2014). In the 1920s, an initial masonry arch dam was built in Valgrosina, which in 1960 was replaced by a spur and gravity-relieved dam further upstream in correspondence to the closing section of the Eita Valley (A2A S.p.A. 1954, 1956, 1990, 1990, 1990, 2010). The dam directly collects water from the Eita stream and, through two diversion channels, part of the water from the Sacco stream and the outflow water from the Upper Valtellina hydropower park (Figure 1b). The Valgrosina dam, used for daily modulation of inflow waters, feeds the Grosio power plant downstream.

2.2 | Data Resources

The data used in this study were derived from four main sources: the Regional Environmental Agency of Lombardy (ARPA), Lombardy Region, A2A S.p.A. and MeteoSWISS. The available rainfall data are essentially of two types: measured by rain gauges or obtained from radar estimates. The 22 stations (tipping bucket rain gauges) selected within a 25-km radius buffer zone centered on the study area provide hourly precipitation values and they belong to three different monitoring networks (Figure 2): the Regional Environmental Agency ARPA, the A2A hydroelectric company, and the Swiss meteorological service MeteoSWISS. Data were collected for the period October 2010 to September 2020 (10 hydrologic years, from 1 October to 30 September of the following year). Within the study area there are three stations, one from ARPA and two from the A2A company. The other 19 are arranged around the area of interest. All weather stations are also equipped with thermometers at 2 m above the ground, recording hourly (Figure 2, from point A to V).

Regarding radar data, the CombiPrecip dataset is a ground-based weather radar–rain gauge composite at 1-km horizontal resolution. MeteoSWISS provides these data in raster form (.gif) as hourly aggregated radar precipitation estimates (Swiss coordinates EPSG: 21781) (Germann et al. 2006; Sideris, Gabella, Erdin and Germann, 2014, 2014). Within the Swiss territory, the rain gauges series and the radar values at the same locations are retrieved to be used as input for the geostatistical algorithm (co-kriging with external drift) that generates the composite dataset (Sideris, Gabella, Erdin and Germann, 2014, 2014). The quality of the composite dataset decreases as the distance from a rain gauge location increases. This situation does not affect the general quality of the dataset within the Swiss territory (evaluated only for Switzerland in Sideris et al. (2014)), but it is expected to affect it in areas outside the Swiss border since information from the ground-based

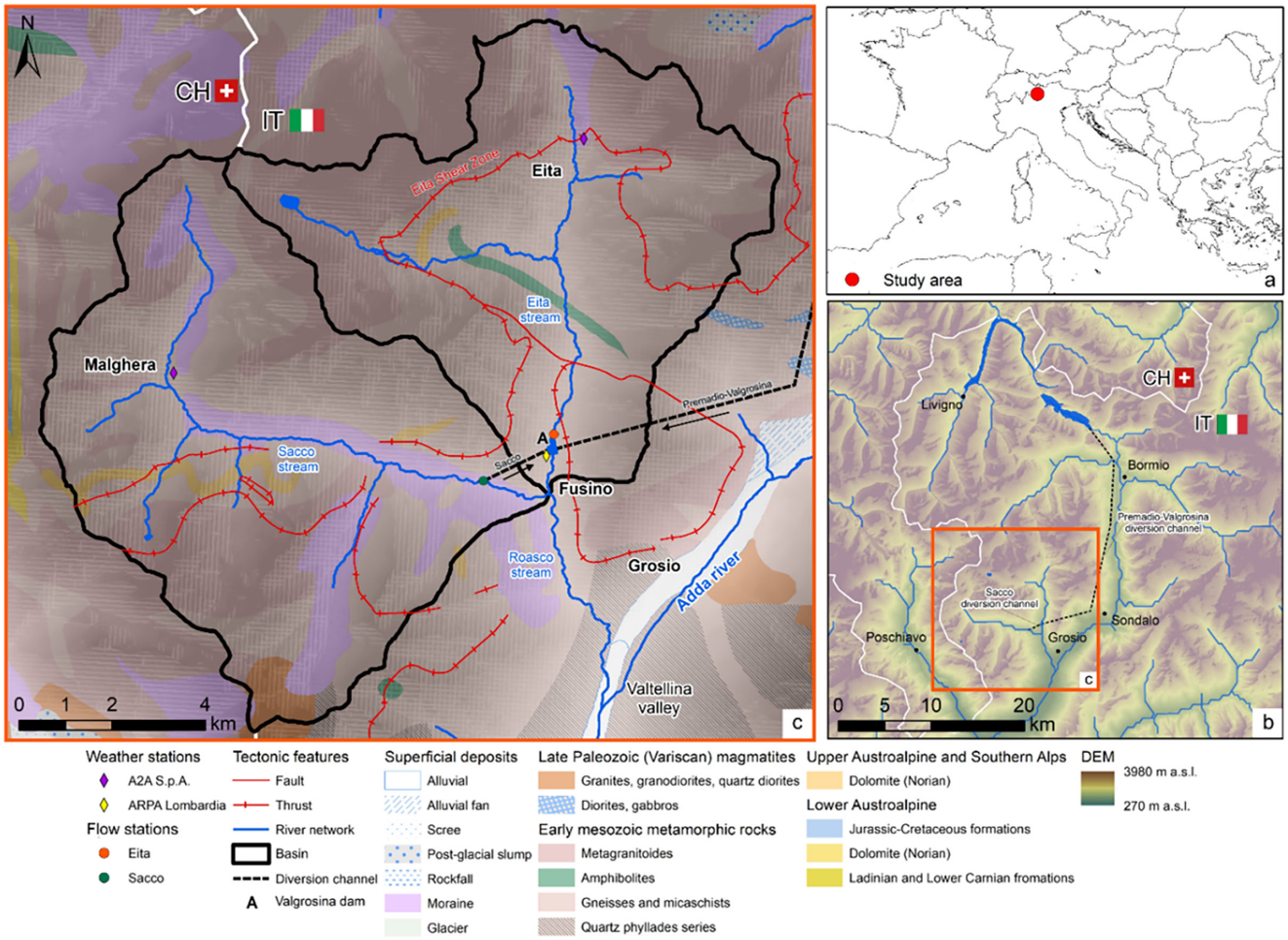

FIGURE 1 | (a) Location of the study area within south-central Europe, (b) geographical focus on the Alta Valtellina and tracks of the two diversion channels involved, and (c) geological context of the study area derived from the Geological Map of Switzerland 1:500.000 (University of Bern–Institute of Geology and Federal Office for Water and Geology 2005).

monitoring network is not acquired. Essentially, at some distance from the border the influence of the ground-based data is zero and the data is raw radar. This method has been used operationally since 2012 by the Swiss weather service (Sideris, Gabella, Erdin and Germann, 2014, 2014). There is a value that varies from 0 to 255 in each pixel and these values can be converted to a minimum, mean, and maximum precipitation intensity. The radar acquisition is generated every 5 min based on a combination of the data of the available radars over Switzerland (Figure 2).

In addition to the meteorological variables, the digital elevation model (DEM) at 20 × 20 m resolution obtained from the Lombardy Region geoportal (www.geoportale.regione.lombardia.it) and the datasets of the in-flow discharge (m^3s^{-1}) into the artificial reservoir were used to conduct the study. Hourly discharge rates were made available by A2A at the flow stations of the Eita stream just upstream of the dam-lake and at the inlet of the diversion canal from the Sacco stream to the dam-lake, and cover the October 2010–September 2020 period. Furthermore, minimum environmental flow (MEF) values of the Sacco stream (0.266 m^3s^{-1} in the summer season and 0.406 m^3s^{-1} in the winter season) were added to the Sacco diversion canal flows for the calibration of the Sacco basin (see Section 2.3.4).

2.3 | Methods

The workflow can be divided into three main steps: (i) the hourly CombiPrecip data (henceforth "radar data") were corrected with rain gauge values by applying two point-based (Sections 2.3.1 and 2.3.2) and four spatial (Section 2.3.3) correction approaches; (ii) the hydrologic model was fed in each sub-basin centroid (see Section 2.3.4) by the corrected precipitation series and calibrated for the study area and (iii) the performances of both the precipitation corrections and the simulated hydrologic responses were evaluated. Among these two correction approaches, the point-based methods present the advantage of a possible application for both "historical" (observed) data (e.g., Vogl et al. (2012)) and "future" data such as nowcasts (e.g., Shehu and Haberlandt (2021) and Yazdandoost et al. (2020)). The spatial approach can be applied only to correct observed radar data since they always require the simultaneous knowledge of ground (rain gauges) records. In this study, both correction approaches were evaluated in relation to a simple Triangular Irregular Network (TIN) interpolation, the OK interpolation of the rain gauge data, and the raw radar data. The latter were considered as the benchmark dataset. Acronyms related to the datasets investigated and referred to hereafter are given in Table 1.

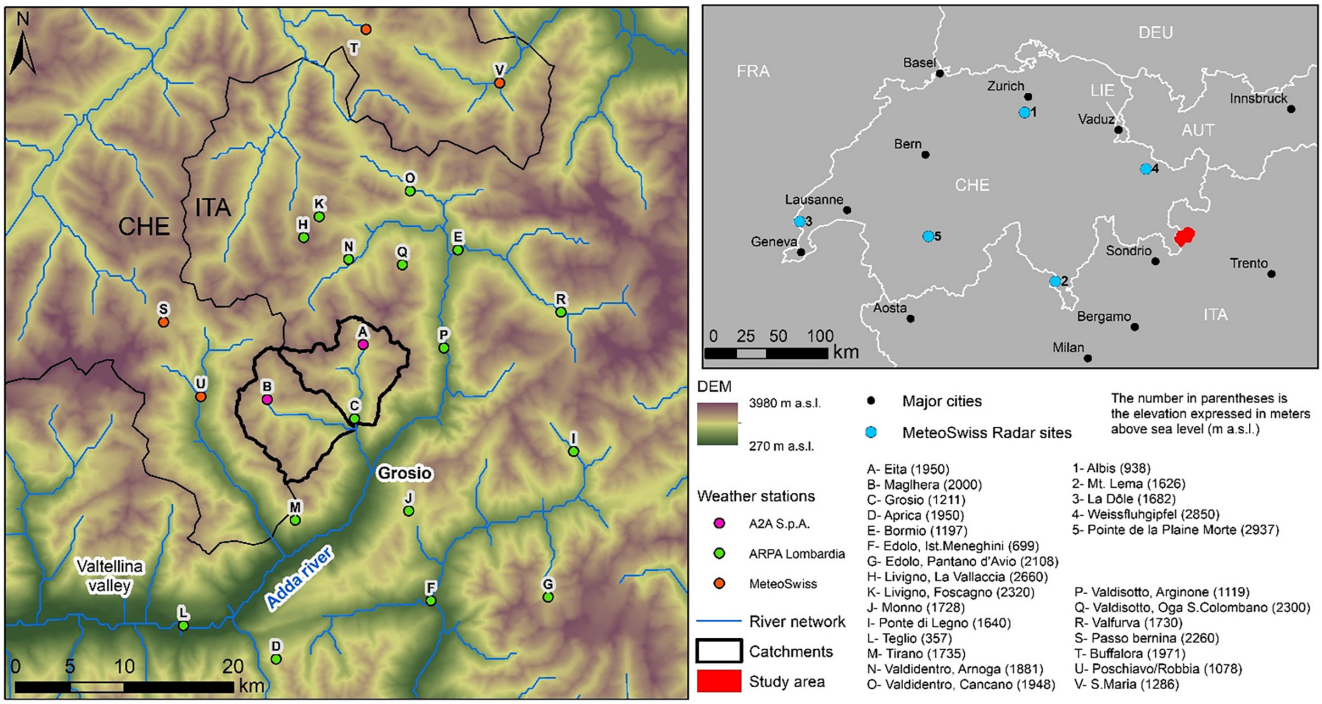

FIGURE 2 | Location of the 22 weather stations used and radar stations on Swiss territory. The legend indicates the altitude of the stations in m a.s.l. in parentheses.

TABLE 1 | Acronyms of the investigated datasets.

Acronym	Approach	Explanation
Raw radar data	Benchmark	Raw radar data dataset
Rain gauge TIN	—	Triangular irregular network interpolation of the rain gauge data
Rain gauge OK	—	Interpolation of rain gauge data according to ordinary kriging
TIN-Copula	Point-based	Copula correction based on a triangular irregular network
TIN-CDF	Point-based	Cumulative distribution unction correction based on a triangular irregular network
Radar + IDW	Spatial (deterministic)	Radar data as a trend and inverse distance weighting on the residuals
Radar + TPS	Spatial (deterministic)	Radar data as a trend and Thin Plate Spline on the residuals
Radar + OK	Spatial (geostatistical)	Radar data as a trend and ordinary kriging on the residuals
Radar + DK	Spatial (geostatistical)	Radar data as a trend and detrended kriging on the residuals

2.3.1 | TIN Interpolation

To obtain the rainfall amount from the gauges at the sub-basin centroids, the study area is subdivided into a TIN considering the rain gauges as nodes and performing a Delaunay triangulation (Delaunay 1934; Lazoglou, Gräler, and Anagnostopoulou 2019; Renka et al. 2020). This triangulation prevents other nodes (rain gauges) other than the vertices of a triangle from being inside the circumcircle defined by the triangle itself, avoiding sliver triangles (Figure 3a,b). For each triangle, three weight coefficients are derived by dividing the sum of the distances by the centroid-vertex distance:

$$k_j = \frac{\sum d_i}{d_j \cdot \left(\frac{\sum d_i}{d_a} + \frac{\sum d_i}{d_b} + \frac{\sum d_i}{d_c} \right)} \quad (1)$$

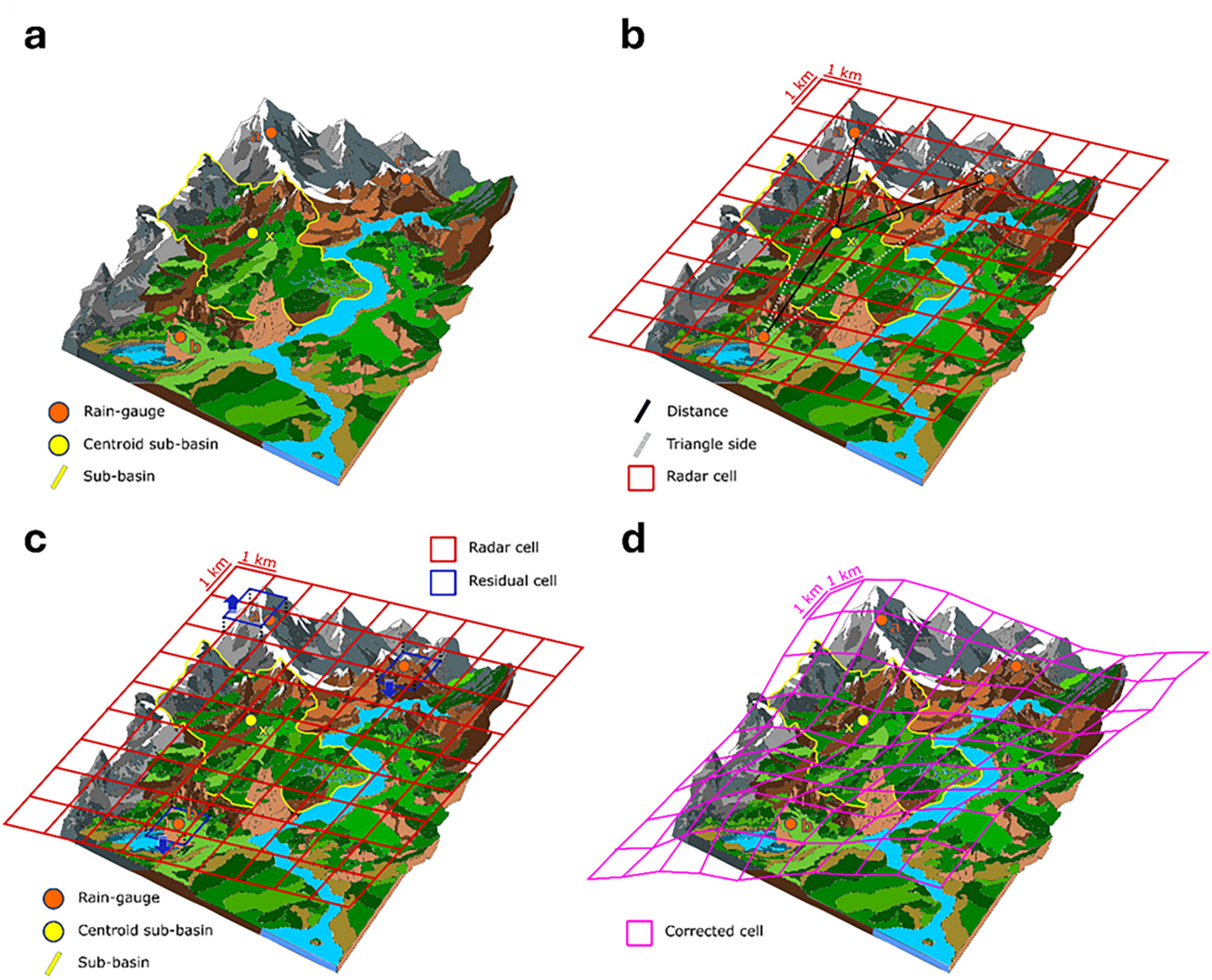

FIGURE 3 | (a) An example of a typical alpine environment with three weather stations (a–c) at different elevations. (b) In this situation, radar values from the cells corresponding to stations a, b and c are used to correct the X centroid by exploiting a TIN. (c) Differences between rain gauge values and corresponding radar cells are calculated. (d) The corrected surface is obtained from the cell-by-cell algebraic sum between radar values and spatial interpolation on the residuals.

where k denotes the weight coefficient of gauge j (a, b or c), d the centroid-vertex distances, and i represent all three gauge indices (a, b and c). This equation implies that the closer the gauge is to the centroid, the more weight its coefficient will have since the sum of the three coefficients (a, b and c) is equal to 1. Once the TIN is defined (Figure 3b), P_X precipitation at the centroid X (rain gauge TIN dataset) for each timestep can be computed as follows:

$$P_X = k_a P_a + k_b P_b + k_c P_c \quad (2)$$

where $k_{a,b,c}$ represent the three coefficients defined for each sub-basin centroid triangle by Equation (1) and $P_{a,b,c}$ are the hourly precipitation value at the rain gauge a, b and c, respectively.

2.3.2 | Copula and CDF Techniques

In the case of the point-based approach, the first step consists of extracting the hourly precipitation series from the radar data (October 2010–September 2020) of the 1-km^2 cells where the centroids are located (Figure 3b). These radar data series are adjusted taking into account only values greater than 0.2 mm/h, which is the detection limit of rain gauges.

In the second step, two statistical techniques are performed: Copula and Cumulative Distribution Function (CDF) techniques. For each of the three rain gauges-centroid comparisons, the hourly time series of positive pairs were obtained. The term "positive pairs" means precipitation values greater than 0.2 mm/h for both observed and radar data in each timestep following the suggestion of Foehn et al. (2018) but with a case study-specific limit of detectability. For each target triangle, in the vertex-centroid comparison, the bivariate copula families that best describe the dependence between each rain gauge and radar data pair were tested and the best one according to the largest Akaike information criterion (AIC) value (Akaike 1974) was selected. Gamma, log-normal and Weibull distributions were tested, as the most common distributions for describing precipitation timeseries. The hourly values at the

centroids were derived from the hourly values obtained from the copula corrections with Equation (2) (in this case, $P_{a,b,c}$ are the hourly corrected precipitation value at the rain gauge a, b and c, respectively).

Likewise, based on positive pairs, the CDF matching bias correction method was tested. As explained by Reichle and Koster (2004) in a study where satellite soil moisture data were corrected with those from a land surface model, the idea is to reduce the bias by matching the CDF of the rain gauge and radar data. The x' corrected radar data are then obtained by the formula:

$$CDF_{obs}(x') = CDF_{rad}(x) \tag{3}$$

where CDF_{rad} and CDF_{obs} denote the CDF's of the radar and rain gauge precipitation values, respectively, and x is the unscaled radar value. The code in MATLAB by Singh (2022) was used for the application of this technique. Also, for this technique, the corrected series at the centroid location was finally obtained through Equation (2).

2.3.3 | Spatial Radar Corrections

Spatial correction aims to correct the radar values by spatially interpolating the error between the rain gauges and the corresponding radar cell (Borga et al. 2002; Cecinati, Wani, and Rico-Ramirez 2017; Delrieu et al. 2014). This approach was implemented in three steps:

- The residuals, namely the differences between the hourly radar values and the rain gauge values, in the radar cells where a rain gauge is located (Figure 3c), were calculated.
- The error field (residuals) was interpolated by applying different deterministic and geostatistical algorithms.
- The interpolation was combined with the radar trend in each cell, and finally, the corrected surface was obtained by setting values below the detection limit to zero (Figure 3d).

In this study, two deterministic techniques, namely IDW and thin plate spline (TPS), and two geostatistical techniques, namely OK and Detrended Kriging (DK), were tested on the residuals.

The IDW interpolation (Shepard 1968) assigns a target point a value given by the weighted average of known values located in its proximity (Gilewski 2021). With the condition that the sum is equal to one, the weight coefficients are defined by the inverse of the distance and normalised. The TPS interpolation represents a data-oriented, non-parametric technique involving locally weighted polynomial procedures (Duchon 1977). From the initial dataset, the TPS allows the interpolated surface to pass as neatly as possible close to the known points by minimising differences through a smoothing procedure. These two deterministic methods were performed on the residuals through the use of two packages in the R environment, "idw" in the "gstat" package (Gräler, Pebesma, and Heuvelink 2016; Pebesma 2004) and "Tps" in the "fields" package (Nychka et al. 2017), respectively. The "Tps" package allows the automatic setting of the smoothing parameter (lambda) through an internal estimation procedure based on the data provided for each time step (generalised cross-validation).

Geostatistical interpolations on the residuals were carried out with the Spatial Interpolation Kriging package (SIK), a routine of the GEOframe model, exhaustively described in Bancheri et al. (2018). Specifically, OK addresses variations in the local mean by confining stationarity to the nearby area, where the mean remains uncertain; and DK recognises the variations of the local mean within the immediate neighbourhood also exploiting a trend model. Since the trend is defined by an auxiliary variable, the elevation of rain gauges was used in the application of the method (rain gauge elevation values can be seen in Figure 2 legend). Finally, the new corrected precipitation datasets at model input locations (sub-basin centroids) were obtained by extracting the values in the corresponding cells for the raw radar values and from the corrected surfaces using the spatial approaches.

2.3.4 | Hydrologic Model

The GEOframe model (Bancheri 2017; Bancheri, Rigon, and Manfreda 2020; Formetta et al. 2014) was selected to simulate the streamflow. GEOframe is a semi-distributed, component-based hydrologic system. It includes several components that individually simulate the physical processes of the hydrologic cycle in a sequence. These assembled components reproduce the surface runoff and hydrologic response of the catchment from hourly meteorological, rainfall and hydrometric data. The study area is divided into a series of sub-basins, for which the model solves the hydrologic budget and finally connects the individual units to obtain the overall response of the entire catchment.

The model is developed in four main steps. First, starting from the DEM, a geomorphological analysis is carried out that returns the sub-basins and their centroids. This analysis considers several features including river network characteristics, total contributing area values and drain direction. Second, the data series of temperature and precipitation, with the temporal resolution of interest, are obtained at each sub-basin centroid by interpolation of station-based data and, through internal routines, the radiation and evapotranspiration series are calculated. The model allows the interpolation phase to be by-passed if externally obtained spatial dataset are available. Third, the hydrologic components are computed in each sub-basin centroid (Bancheri, Rigon, and Manfreda 2020). Interacting with each other, these components provide the delay time and the amount of water discharged to the sub-basin outlet. The components are governed by mathematical equations that describe, in a simplified form, the phases of the hydrologic cycle and are schematized in the snowpack, canopy layer, root zone, direct runoff and groundwater storage (Figure A1). Finally, the streamflow at the closure section is simulated following the topology scheme that considers the upstream-downstream relations to connect the sub-basins.

The discretization of the study area into sub-basins was carried out using the geomorphological analysis routine of GEOframe. The 20×20 m DEM was the only input in this first step and a surface threshold of 2.5 km^2 was used for the delineation of the sub-basins. The outlets of the two basins were placed at the flow stations at the inflow to the dam (Eita) and at the diversion channel inlet (Sacco). For each of the sub-basin centroids, GEOframe components were run to obtain the hourly values of temperature (through DK interpolation), evapotranspiration (Priestley and Taylor 1972), and radiation, by applying the Idso model (Idso 1981). The precipitation was divided into snow and rain using the Hock's model (Hock 1999).

In the GEOframe environment, it is possible to calibrate 17 parameters, which are listed in Table 2 with their suggested ranges (Bancheri 2017). The α_r and α_s coefficients allow correction for the amount of liquid and solid precipitation entering the system since the input represents only the centroid of the sub-basin value and not a spatial average of the entire sub-basin. The Melting temperature, Combined Melting factor and α_l coefficient give the amount and rate of snowmelt for each timestep, while the Kc and p coefficients govern the amount of water reaching the soil from the canopy layer and the pB soil factor gives the value of the moisture content. The three storages (Root zone, Runoff and Groundwater) are governed by three factors each: a maximum storage value (in mm), a coefficient (g, c and e, respectively) that gives an estimate of the discharge delay, and an exponent (h, d and f, respectively) responsible for the shape/slope of the discharge curve. The last two factors are dimensionless.

Model calibration was carried out through a stepwise multiple-objective and automated procedure, based on a Shuffled Complex Evolution algorithm (Duan, Gupta, and Sorooshian 1993) ran in a defined parameters space and a Goodness of Fit function (in this case Kling–Gupta efficiency, KGE) that reports the performance of the model. One set of coefficients was derived for each basin (Sacco and Eita).

TABLE 2 | Parameters and their suggested ranges, according to (Bancheri 2017), to be calibrated in the GEOframe model.

Parameter	Unit	Suggested range	Description
α_r	—	0.8 ÷ 1.2	Adjustment coefficient for the rainfall measurement errors
α_s	—	0.5 ÷ 1.2	Adjustment coefficient for the snow measurement errors
Melting temperature	°C	−1.0 ÷ 0.5	Melting temperature
Combined melting factor	mm/°C/h	0.001 ÷ 1	Melting factor
α_l	—	0.3 ÷ 0.9	Coefficient for the computation of the maximum liquid water
kc	—	0.1 ÷ 0.9	Coefficient canopy out
p	—	0.1 ÷ 0.9	Partitioning coefficient free throughfall
s_RootZoneMax	mm	10 ÷ 200	Maximum value of the rootzone water storage
g	—	0.01 ÷ 10	Coefficient of maximum percolation rate
h	—	1 ÷ 3	Exponent of non-linear root zone reservoir model
pB_soil	—	0.2 ÷ 3	Degree of spatial variability of the soil moisture capacity
s_RunoffMax	mm	10 ÷ 200	Maximum runoff storage
c	—	1 ÷ 50	Coefficient of the non-linear runoff reservoir model
d	—	1 ÷ 3	Exponent of the non-linear runoff reservoir model
s_GroundWaterMax	mm	50 ÷ 300	Maximum groundwater storage
e	—	0.001 ÷ 10	Coefficient of the non-linear groundwater reservoir model
f	—	1 ÷ 3	Exponent of the non-linear groundwater reservoir model

2.3.5 | Evaluation of Radar Corrections

To evaluate the radar correction, the corrected series were cross-validated by performing the leave one out test (LOO) (Bancheri et al. 2018). For the spatial approach, the cross-validation involves a process where individual data points are taken out one by one, and the interpolation is conducted using the remaining stations (GEOframe-SIK routine for geostatistical methods and a R script for the deterministic ones). Regarding the point-based procedure, LOO tests were carried out by pretending to correct a radar cell where a rain gauge is located. This process involves recalculating the TIN for each rain gauge, including the location of the rain gauge to be evaluated in the target triangle area on which the weighted coefficients will be obtained for the evaluation. Due to these conditions, some boundary weather stations will not be eligible for cross-validation (6 out of 22 rain gauges). For this reason, the comparison of all tested datasets will be presented only for the common 14 weather stations (14WS). For the evaluation of the radar correction, five performance criteria, described in the following text, were calculated.

The KGE (Gupta et al. 2009; Kling, Fuchs, and Paulin 2012) was used to evaluate the radar correction. The KGE represents how far the correction performance deviates from the ideal point in a space defined by its three constituent elements: correlation (r namely the Pearson correlation coefficient), variability bias (γ) and mean bias (β).

$$\mathrm{KGE} = 1 - \sqrt{(r-1)^2 + (\beta-1)^2 + (\gamma-1)^2} \tag{4}$$

$$\beta = \frac{\mu_{SIM}}{\mu_{OBS}} \tag{5}$$

$$\gamma = \frac{\sigma_{\mathrm{SIM}} / \mu_{\mathrm{SIM}}}{\sigma_{\mathrm{OBS}/\mu_{\mathrm{OBS}}}} \tag{6}$$

where OBS and SIM denote the observed precipitation recorded at the rain gauge and the corrected radar series, respectively, μ represents the mean precipitation, and σ the precipitation standard deviation. This index ranges from 1 to minus infinity, where 1 indicates the perfect match between the observed and the corrected series. KGE values greater than 0.75 are considered as highly acceptable (Towner et al. 2019), in contrast, values less than 0.50 are not considered optimal (Andersson et al. 2017).

The Nash–Sutcliffe efficiency index NSE (Nash and Sutcliffe 1970) was also calculated. Given the number of observations from $i = 1$ to n (the total) and the corrected values corresponding to the same timestep, the NSE index is defined as:

$$\mathrm{NSE} = 1 - \frac{\sum_{i=1}^{n} \left(\mathrm{OBS}_i - \mathrm{SIM}_i\right)^2}{\sum_{i=1}^{n} \left(\mathrm{OBS}_i - \overline{\overline{\mathrm{OBS}}}\right)^2} \tag{7}$$

The root mean square error (RMSE) to provide a complete overview of the distribution of errors (Chai and Draxler 2014):

$$\mathrm{RMSE} = \sqrt{\frac{1}{n} \sum_{i=1}^{n} \left(\mathrm{OBS}_i - \mathrm{SIM}_i\right)^2} \tag{8}$$

The percentage bias (PBIAS) was also considered. Like the former, it measures the average tendency of the simulated values to be larger or smaller than their observed ones, but it is expressed in percentage. Negative values indicate model underestimation, while positive values indicate overestimation:

$$\mathrm{PBIAS} = 100 \frac{\sum_{i=1}^{n} \left(\mathrm{SIM}_i - \mathrm{OBS}_i\right)}{\sum_{i=1}^{n} \mathrm{OBS}_i} \tag{9}$$

The closer the RMSE and PBIAS are to zero, the better the correction is.

TABLE 3 | Hydrological signatures for the discharge evaluation.

Hydrological signatures	Parameter name	Description
Mean winter discharge	Qmean winter	Mean daily discharge (from October to March)
Mean summer discharge	Qmean summer	Mean daily discharge (from April to September)
Runoff ratio	Ratio Q/P	Runoff ratio (ratio of mean daily discharge to mean daily precipitation)
Slope of the flow duration curve	slopeFDC	Slope of the flow duration curve considering the log-transformed 33rd and 66th streamflow percentiles
Baseflow index	BFI	Ratio of mean daily baseflow to mean daily discharge, hydrograph separation performed using Ladson et al. (2013) digital filter
Mean half-flow date	HFDmean	Julian day on which the cumulative discharge since 1 October reaches half of the annual discharge
Low-fow	Q5	5% Flow quantile
High-flow	Q95	95% Flow quantile
Frequency of days below threshold	05Q freq	Frequency of days with $Q < 0.5\,m^3\,day^{-1}$

In the specific case of hourly radar corrections, the composite scaled score (CSS) proposed by Sofokleous et al. (2021) was calculated to better rank the correction methods applied. This index combines into a single score the values of KGE, RMSE and two deterministic verification scores: the extreme event score, EES (Sofokleous et al. 2021) and the Peirce skill score, PSS (Peirce 1884). The latter skill scores are based on the combination of hit rate (H) and frequency bias (fBIAS), which are themselves obtained according to a 2×2 contingency table that allows for each timestep to count hits (positive pairs—OBS and SIM events), false positives (only SIM event), misses (only OBS event) and correct non-events (both no events). For this case study, the CSS index was calculated according to this formula:

$$\mathrm{CSS}_j = \frac{1}{N_s}\sum_{s=1}^{N_s}\left(\frac{x_{s,j} - x_{s,\mathrm{worst}}}{x_{s,\mathrm{best}} - x_{s,\mathrm{worst}}}\right) \tag{10}$$

where j is the index that identifies the tested correction method, s represents the index of the four statistical measures ($N_s = 4$), $x_{s,j}$ is the values of the measure s from the correction method j, and $x_{s,\mathrm{worst}}$ and $x_{s,\mathrm{best}}$ are the worst and the best values, respectively, obtained for the measure s considering all tested methods (Table 1). Only datasets with a CSS value greater than the benchmark were considered for the hydrologic simulation step.

2.3.6 | Assessment of the Hydrologic Model Performance

The evaluation of the hourly hydrologic simulations was done by comparing the observed discharge with those simulated with the different precipitation datasets with which the model was forced. In this study, a spin-up year was considered between October 2010 and September 2011. The calibration period was between October 2011 and March 2016, and the validation phase was between April 2016 and September 2020. KGE, NSE, RMSE and PBIAS were computed similarly to the radar correction. In addition, the logarithmic NSE (lnNSE) was calculated, because it gives more weight to low flows than the NSE (Krause, Boyle, and Bäse 2005). As with the evaluation of the datasets, the CSS index was exploited to compare the performance of the hydrological model for the tested rainfall series taking into consideration the scaled KGE, RMSE, lnNSE and PBIAS values.

Besides the goodness-of-fit indicators for hydrologic model performance derived under calibration and validation phases, other indices characterising the general hydrologic behaviour (hydrological signatures) were evaluated over the entire available period from October 2011 to September 2020. Following the approach of Addor et al. (2018), nine hydrological signatures were selected by modifying them considering their relevance for this case study (Table 3). For the low flow threshold (05Q freq), a value of 0.5 m^3s^{-1} was selected to account for the limitations given by adding the MEF to the Sacco discharge series (see Section 2.2). These indices were calculated on the records obtained through streamflow simulations forced with the tested rainfall datasets and then compared with those obtained from the observed discharge with the coefficient of determination (R^2).

TABLE 4 | Hourly LOO cross-validation results for the 14 available weather station (14WS) for the investigated datasets (see Table 1 for acronyms) over the period October 2010–September 2020.

	14WS							
	Raw radar data	**Rain gauge TIN**	**Rain Gauge OK**	**TIN-copula**	**TIN-CDF**	**Radar + IDW**	**Radar + TPS**	**Radar + OK**	**Radar + DK**
KGE	0.31	0.58	0.21	0.33	0.42	0.51	0.41	0.51	0.49
NSE	−0.08	0.42	0.18	−0.32	−0.11	0.22	0.02	0.36	0.16
RMSE (mm)	0.64	0.75	0.58	0.69	0.64	0.54	0.60	0.44	0.56
PBIAS (%)	−25.78	0.47	−27.49	18.51	−6.52	5.76	27.83	15.60	14.19
Mean annual precipitation (mm)	719	968	765	1144	911	980	1181	881	1061

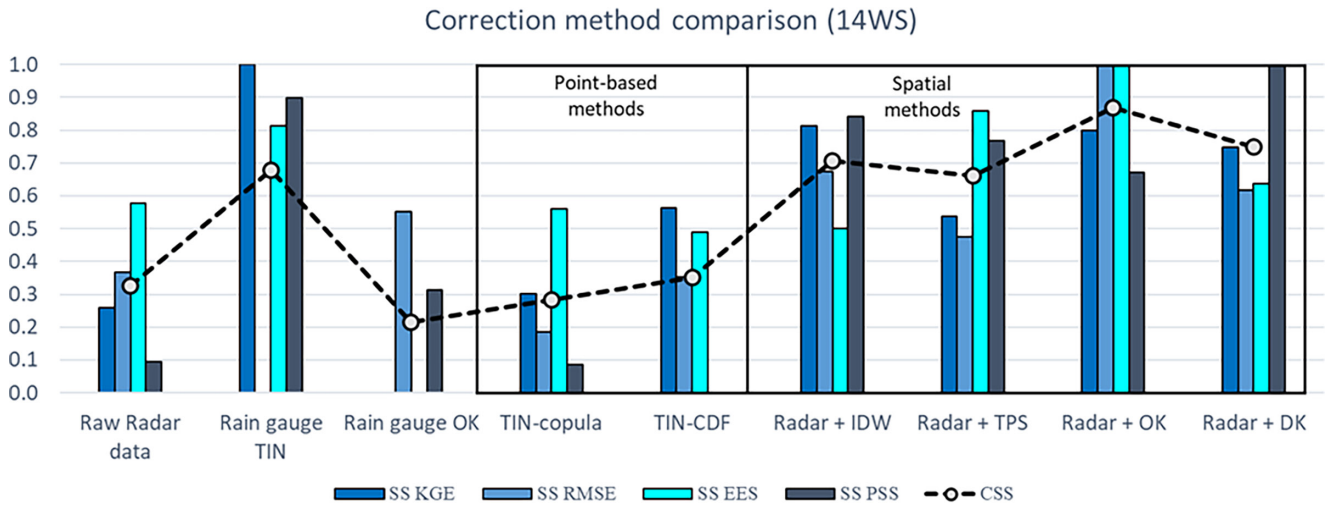

FIGURE 4 | CSS values for all the tested datasets (refer to Table 1) considering the 14 stations in common. The distribution of scaled scores SS combined into the CSS index for each correction method considered is also presented.

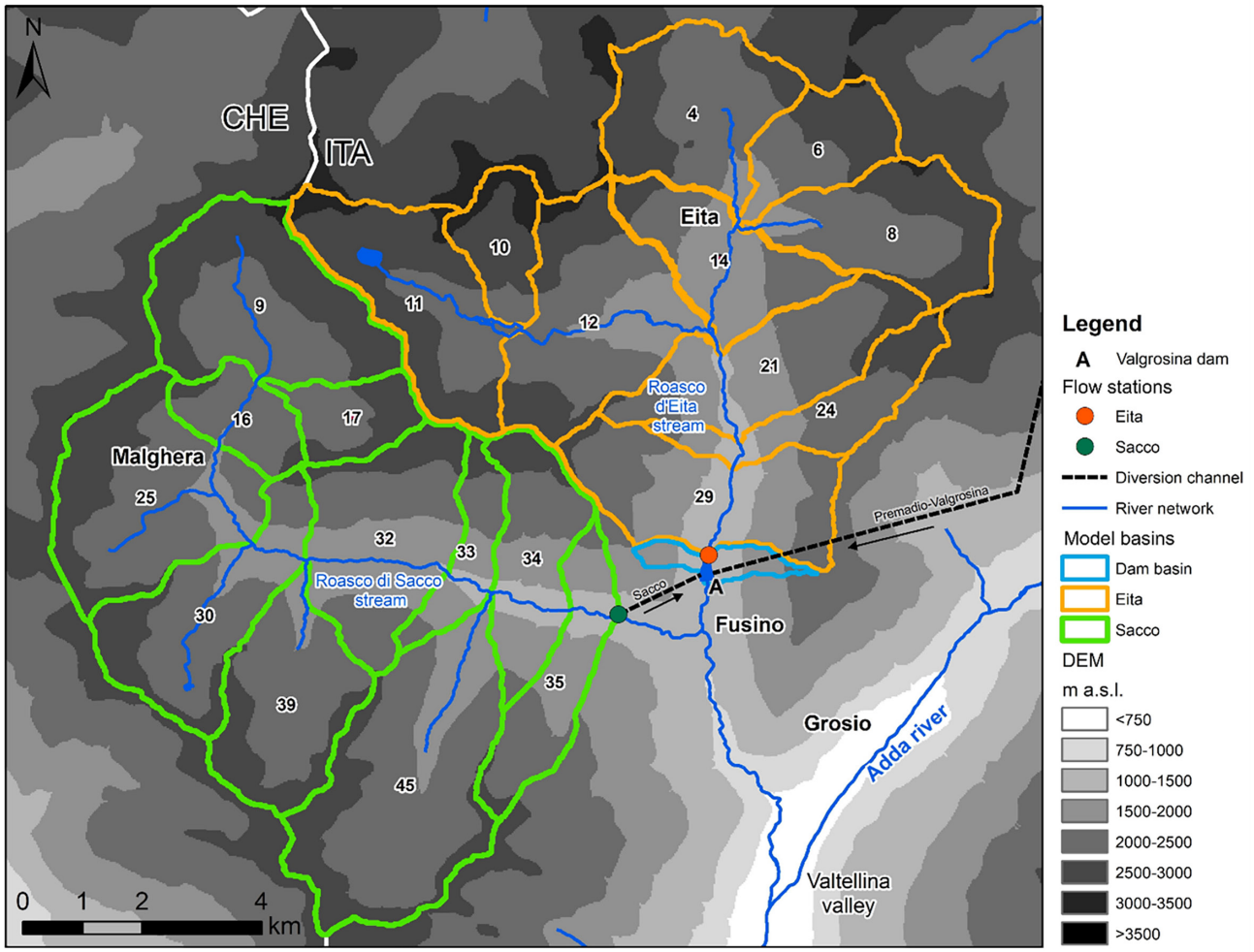

FIGURE 5 | The 21 sub-basins and their corresponding centroids (whose location is indicated by the number label).

3 | Results

3.1 | Radar Correction

The results of the LOO cross-validation test in terms of performance metrics (KGE, NSE, RMSE PBIAS), and mean annual precipitation values are shown in Table 4 for all the tested datasets. These results show the values for the 14 weather stations on which the test could be performed (14WS) for all applied methods. The rain gauge network mean annual precipitation for 14WS is equal to 1230 and 962 mm/y. In this case study, the need for the radar data correction process is supported by the

TABLE 5 | Hydrologic simulation results for the Sacco and Eita basins regarding the calibration (from 2011-10-01 to 2016-03-31) and the validation phases (from 2016-04-01 to 2020-09-30).

	Calibration phase (from 2011-10-01 to 2016-03-31)						
Sacco basin	**Raw radar data**	**Rain gauge TIN**	**TIN-CDF**	**Radar + IDW**	**Radar + TPS**	**Radar + OK**	**Radar + DK**
KGE	0.71	0.71	0.77	0.77	0.75	0.79	0.75
NSE	0.61	0.67	0.64	0.60	0.55	0.59	0.53
lnNSE	−0.20	0.71	−0.25	−0.07	−0.24	0.25	0.10
RMSE (m^3s^{-1})	1.42	1.30	1.36	1.45	1.52	1.46	1.57
PBIAS (%)	−18.70	−6.20	−11.00	−4.70	−8.50	−1.90	−6.60
	Validation phase (from 2016-04-01 to 2020-09-30)						
Sacco basin	**Raw radar data**	**Rain gauge TIN**	**TIN-CDF**	**Radar + IDW**	**Radar + TPS**	**Radar + OK**	**Radar + DK**
KGE	0.73	0.67	0.71	0.77	0.75	0.75	0.71
NSE	0.47	0.40	0.55	0.59	0.51	0.59	0.40
lnNSE	−0.08	0.50	−0.18	0.22	−0.05	0.35	0.17
RMSE (m^3s^{-1})	1.57	1.66	1.44	1.38	1.51	1.37	1.66
PBIAS (%)	10.30	11.60	18.80	12.70	6.40	13.90	6.40
	Calibration phase (from 2011-10-01 to 2016-03-31)						
Eita basin	**Raw radar data**	**Rain gauge TIN**	**TIN-CDF**	**Radar + IDW**	**Radar + TPS**	**Radar + OK**	**Radar + DK**
KGE	0.71	0.84	0.76	0.74	0.72	0.79	0.82
NSE	0.61	0.76	0.63	0.55	0.53	0.70	0.66
lnNSE	−0.20	0.81	0.69	0.38	0.62	0.81	0.73
RMSE (m^3s^{-1})	1.42	0.93	1.17	1.28	1.31	1.05	1.11
PBIAS (%)	−18.70	−4.80	−10.20	−4.60	−4.60	−4.60	−3.30
	Validation phase (from 2016-04-01 to 2020-09-30)						
Eita basin	**Raw radar data**	**Rain gauge TIN**	**TIN-CDF**	**Radar + IDW**	**Radar + TPS**	**Radar + OK**	**Radar + DK**
KGE	0.73	0.72	0.71	0.70	0.78	0.76	0.72
NSE	0.47	0.44	0.55	0.42	0.59	0.54	0.44
lnNSE	−0.08	0.18	−0.18	0.45	0.66	0.50	0.18
RMSE (m^3s^{-1})	1.57	1.49	1.44	1.52	1.29	1.35	1.49
PBIAS (%)	10.30	10.40	18.80	10.40	8.10	7.60	10.40

evidence that radar values underestimate observed values in study area by about 20% (annual cumulative values over the 2010–2020 period). The characteristics of triangles and the coefficient values to carry out the LOO test on corrections exploiting TIN are shown in Table A1. The results of the CSS index for the 14 weather stations are shown in Figure 4 and Table A2.

Table 4 and Figure 4 clearly show how the spatial approach outperforms the raw radar data, Rain gauge OK and the point-based datasets in all respects. The high performance of the spatial approach is confirmed by the CSS index, which attests that the Radar + OK correction is the best out of the nine tested data series with a value of 0.87. Despite not employing radar data in its calculation, Rain gauge TIN obtains solid results that are comparable to the spatial approach (CSS = 0.68) and improve on the benchmark dataset (raw radar data).

An advantage of the spatial approach is also its simplicity of application compared with the point-based method. The latter is quite laborious to apply and time-consuming

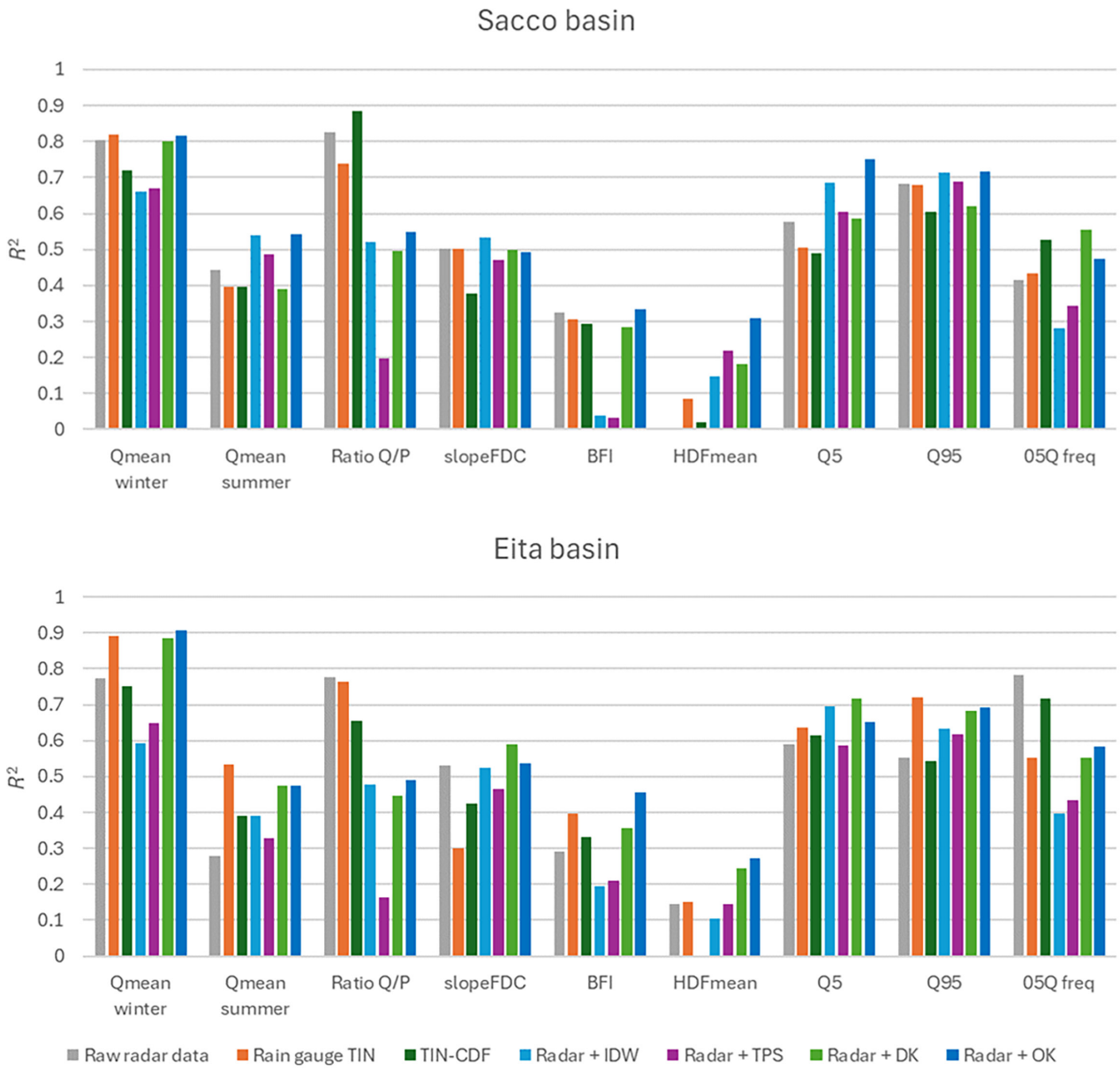

FIGURE 6 | Coefficient of determination (R^2) between the hydrological signatures of the observed and simulated discharges for the two basins (see Table 3 for parameter names).

since it involves an initial phase of extracting the series, then calculating the TIN and weight coefficients, and, finally, the more time-demanding phase where the actual correction is applied and weighted averages are computed. In addition, with this approach, some important spatial pieces of information that the radar data carries are lost. For instance, the spatiotemporal evolution during rainstorm phenomena (Berne and Krajewski 2013; Sokol et al. 2021), which does not have to be interpolated again or reproduced through a TIN but is already provided by the radar resource cell by cell (even though it is not a direct measurement but a processed one). Therefore, even conceptually, the spatial approach proves to be successful because the radar data with all its information and field variations is taken as a trend and corrected at the weather station locations where underestimates or overestimates are found.

3.2 | Hydrologic Model Results

The geomorphological analysis delineated 10 sub-basins in the Eita basin and 11 sub-basins in the Sacco basin (Figure 5). The weather stations that constitute the vertices of the considered triangles and the relative weight coefficients for each sub-basin centroid are displayed in the Table A3. The hydrologic simulation results for the seven precipitation datasets that exceeded the benchmark CSS threshold of 0.33 are presented in Table 5 for the Sacco and Eita basins, respectively. Figure A2 represents the comparison of the two basins by CSS values for both calibration and validation phases while Figure 6 depicts the coefficient of determination (R^2) between the hydrological signatures selected for the tested datasets against the observed streamflow. Also, the ensemble hydrographs are presented in Figure 7 (Sacco) and Figure 8 (Eita),

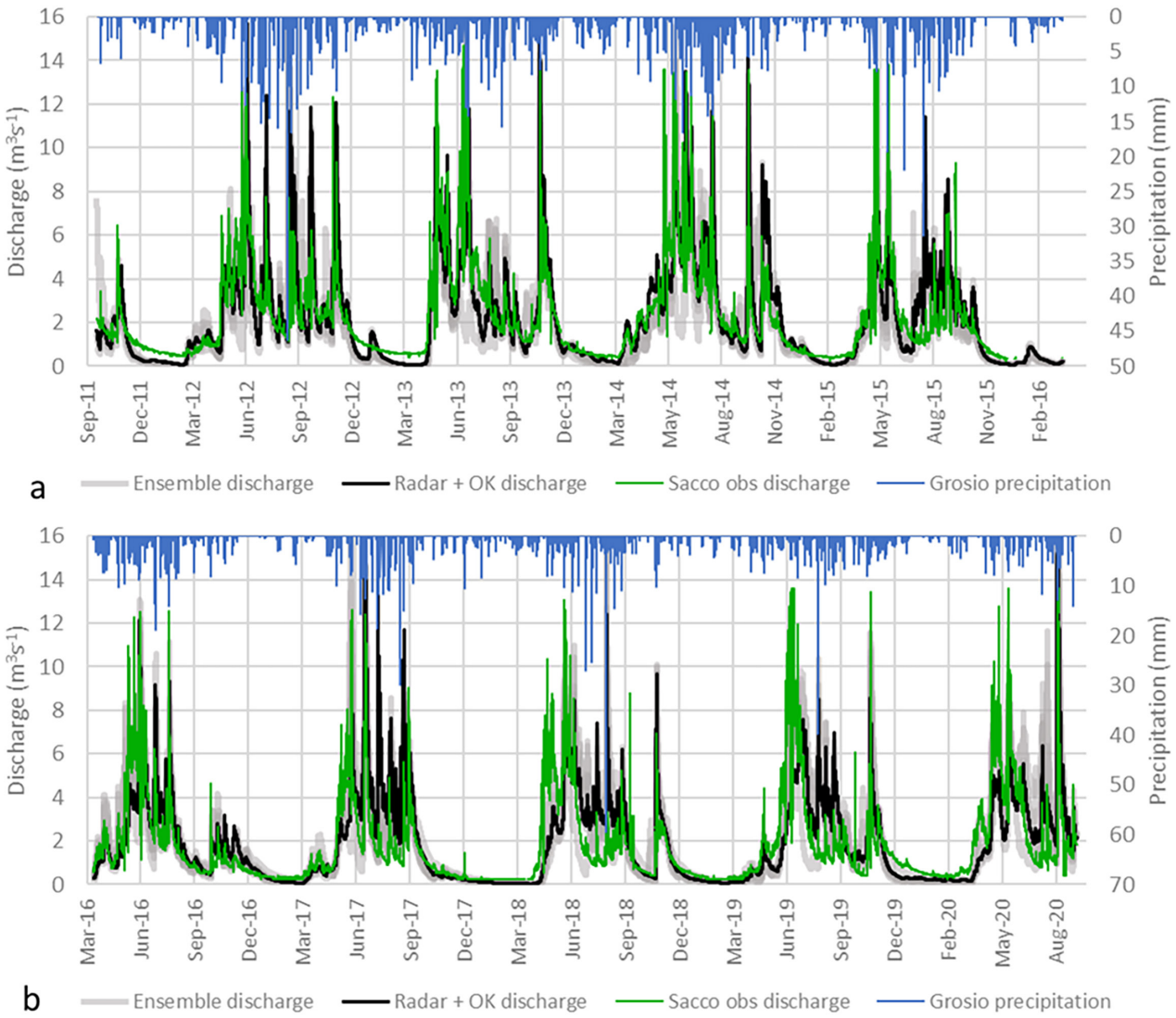

FIGURE 7 | Discharge rates (m^3s^{-1}) for the Sacco basin for (a) the calibration (October 2011–March 2016) and (b) the validation period (April 2016–September 2020) and the precipitation of the Grosio rain gauge (C).

highlighting the results obtained with the most robust dataset (Radar + OK). Tables A4 and A5 show the calibrated parameters for the two basins for the seven precipitation datasets used as input to feed the model.

The hydrologic modelling output confirms the benefit of applying the radar data correction. The best performance is obtained using the Radar + OK and Rain gauge TIN as the precipitation dataset, outperforming the other simulations fed with the other corrected series. Analysing the CSS values for the two branches of the hydrologic model (Figure 6), the average values between the calibration and validation phase relative to the Radar + OK dataset are better than the Rain gauge TIN for Sacco (0.81 vs. 0.67) and slightly higher for Eita as well (0.88 vs. 0.87). Remarkably, the model forced by Radar + OK precipitation data is robust for both basins considered, maintaining in both the calibration and validation phases values of KGE and NSE above 0.75 and 0.59, respectively (Table 5). The hourly analysis of the RMSE and PBIAS values reveals the first weaknesses, with non-negligible RMSE ranging between 1.05 and 1.46 m^3s^{-1}, but not exceeding 14% bias. Even graphically it is possible to notice the error (grey shading in Figures 7 and 8) with higher dispersion in the summer periods (July–August) in comparison to other periods of the year throughout the time series. The low flow behaviour, on the other hand, is well captured, with relatively good hourly lnNSE values for the Radar + OK dataset in the Sacco basin (calibration 0.25—validation 0.35) and very good for the Eita basin (calibration 0.81—validation 0.86). In the specific case of the Sacco branch, the low flow is best captured by the Rain gauge TIN dataset with hourly lnNSE values of 0.71 and 0.50 for calibration and validation, respectively. This situation can be ascribed to uncertainties related to the MEF considered only for the Sacco basin. Finally, regarding the calibrated parameters of the model (Tables A4 and A5), it is interesting to focus on the α correction coefficients for liquid precipitation which in all cases correct the overestimation of precipitation except for the TIN-CDF correction where the volume of water entering the system as precipitation is increased However, this trend does not seem to be related to relative rain differences

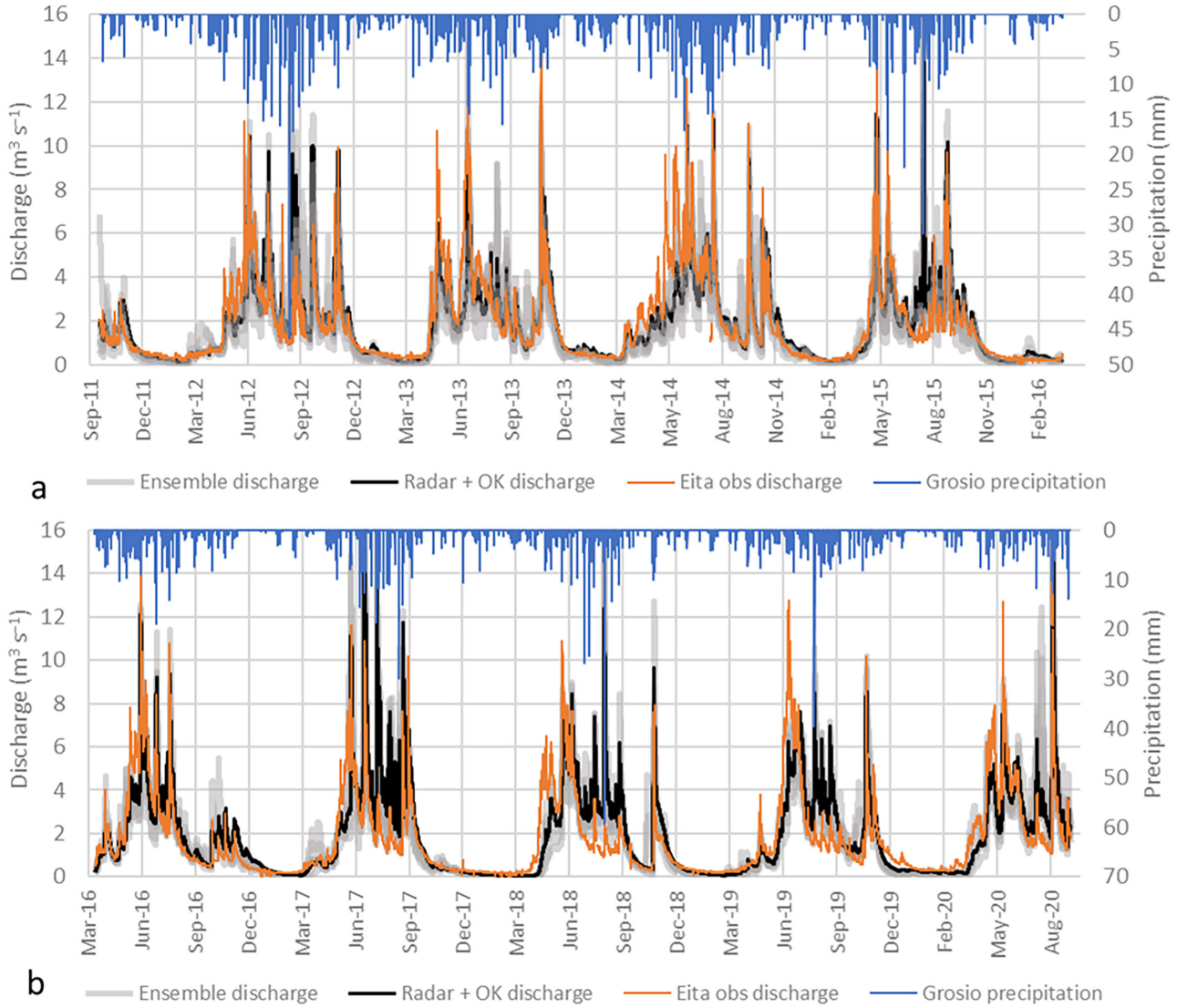

FIGURE 8 | Discharge rates (m^3s^{-1}) for the Eita basin for (a) the calibration (October 2011–March 2016) and (b) the validation period (April 2016–September 2020) and the precipitation of the Grosio rain gauge (C).

in Table 4. The analysis of storage characteristics depicts a typical behaviour of a mountain catchment. The runoff component is characterised by low maximum storage volumes with high response, compared to those of the Root zone and Groundwater components.

Regarding the analysis of hydrological signatures, as shown in Figure 6, the benchmark dataset (Raw radar data) presents relatively good values for many signatures (e.g., on the frequency of values below the threshold of $0.5\,m^3s^{-1}$, 05Q freq) except for the baseflow index (BFI) and the reach of mean half-flow date (HDFmean). The lower values for Qmean summer compared with Qmean winter highlight issues related to the difficulty of correctly simulating snowmelt dynamics. Overall, the Radar + OK dataset performs better than the others with an average R^2 of around 57% for both basins but does exhibit below-average values for BFI and HDFmean, indicating them as weaknesses of the hydrologic model in reproducing this aspect of the hydrologic behaviour of the two basins. The Rain gauge TIN and Radar + DK datasets also show consistently good performance with similar average R^2 values around 50% and 56% for Sacco and Eita, respectively.

4 | Discussion

Many radar adjustments can be found in the literature that combine radar data with rain gauges networks and apply geostatistical techniques (mostly kriging with external drift) to adjust the mean-field bias (e.g., Haberlandt 2007; Seo, Breidenbach, and Johnson 1999; Velasco-Forero et al. 2009; Wang et al. 2013). For instance, in Borga et al. (2002), a correction of the hourly radar signal was successfully applied over an area of the same size as Valgrosina (about $130\,km^2$) focusing on the vertical profile of reflectivity, anomalous propagation of the radar beam, and Mean-Field bias, adjusting an underestimation of about 24% (very close to the 20% of this case study). Likewise the spatial approach applied in this work, in Sinclair, and Pegram. (2005)

radar data were used to refine spatially confined information derived from interpolation between rain gauges performing the Conditional Merging technique (Ehret 2002). This process generates an estimate of the precipitation field that preserves the accurate spatial structure while meeting the constraints imposed by the ground-measurements. The results of the tests conducted in this study support the findings of Thorndahl et al. (2017), namely, that spatial geostatistical approaches appear to be the most advanced among those applied in the research community. A similar approach was applied by Cheng et al. (2017), where different rainfall sets derived from rain gauge-based interpolations were used as input of a hydrologic model. The authors showed that the Principal Component Regression with residual correction technique, which considers the morphological characteristics of the study area such as, for instance, elevation and slope, is the best against deterministic techniques. In this research, no technique that involved the morphological characteristics was tested (except for Radar + DK correction where the elevation of weather stations was considered), because the goal was to find a correction that needed a minimum of data and was improved by the integration of the rain gauge network to increase its operational efficiency. Furthermore, it should be recalled that the radar data used is a product of the application of co-kriging with external drift, calibrated for the Swiss territory and not outside the Swiss borders, where the radar signal is practically raw. A further step of investigation could be to test geostatistical techniques that massively integrate descriptive variables of the morphology of the study area. Using the same modelling approach (GEOframe system) but only by exploiting the interpolation routine embedded in the model (Rain gauge OK in this study) for the meteorological variables (temperature and precipitation), examples can be found applied in southern Italy (Bancheri, Rigon, and Manfreda 2020) and north-eastern Italy (Arnone et al. 2023), under data-scarce conditions in contrast to this case study.

Since spatial methods have a comparable performance in terms of CSS (quality of precipitation data) and model robustness, they could be used collectively as an ensemble to evaluate possible uncertainties in the estimation of the discharge at the dam lake inlet. This potential next step would represent a strategic operational tool by which probabilistic streamflow simulations can be obtained. In detail, if used operationally, these simulations could represent different initial conditions for forecast runs. Also, by defining a water storage threshold level for the dam lake, the ensemble of streamflow simulations can be used to optimise hydropower production in the study area by considering different management scenarios with their associated uncertainties. This represents a crucial factor for integrated reservoir management since it indicates the operational threshold of water availability. Conversely, the point-based methods showed a lower performance compared to the spatial ones and were very complex to develop. Therefore, the added value in including them in such an implementation would be extremely limited. However, considering the comparable performance of the model calibrated with TIN-CDF and the benchmark dataset, the point-based approach showed the potential to be tested by transferring the bias-correction applied on legacy records to nowcast radar data, when available from the same source.

5 | Conclusions

In this study, precipitation data derived from weather radar were corrected based on a network of 22 rain gauges in the Italian Alps, using a point-based and a spatial method. The point-based method exploits a system of TINs and weighted averages. The spatial approach applies deterministic and geostatistical techniques on residuals and then obtains a corrected surface by exploiting the radar value as a trend (Radar + correction on residuals). By LOO cross-validation tests, the observed precipitation series recorded at the 14 common rain gauges were compared with all nine datasets: the raw radar data, precipitation interpolations (Rain gauge TIN and Rain gauge OK), point-based corrections (TIN-copula and TIN-CDF), spatial corrections (Radar + IDW, Radar + TPS, Radar + OK, and Radar + DK). Datasets with a CSS value greater than benchmark precipitation series (raw radar data) were used as input to the semi-distributed GEOFrame hydrologic model and parameters were calibrated.

From both the radar correction and modelling perspectives, the Radar + OK correction emerges the best, outperforming the other datasets with mean KGE with values of 0.51 for precipitation correction and 0.79 and 0.75 for hydrologic model calibration and validation, respectively. Although there are problems in modelling summer periods (average overestimation of 12% for Eita and 18% for Sacco, for the June–September months), forcing the model with the Radar + OK (and Rain gauge TIN) precipitation datasets produced significant improvements in simulating low flows compared with using the other corrected precipitation datasets with mean hourly lnNSE values of 0.30 (0.61) and 0.74 (0.63) considering all the record for Sacco and Eita, respectively. This represents a crucial factor for integrated watershed management because it indicates the operational threshold of water availability.

This study presented two approaches of hourly radar correction techniques that can be improved by adding terrain morphological attributes as co-variates. These results emphasise the potential of exploiting radar data in hydrologic modelling. This not only expands the possibilities of having increasingly accurate and responsive streamflow simulations, but also promotes more resilient management of water resources in this ever-changing field.

Acknowledgements

The authors acknowledge A2A S.p.A. for providing the data necessary for the study conducted as part of the scientific agreement between the company and the University of Milan. Sincere gratitude also is owed to the Erasmus Internship project for providing the financial support to carry out a fundamental part of research at the Cyprus Institute. We wish to acknowledge the Italian Ministry of Education, University and Research (MIUR) that partially supported this work through the project "Dipartimenti di Eccellenza 2023–2027".

Data Availability Statement

The data that support the findings of this study are available from the corresponding author upon reasonable request.

References

A2A S.p.A. 1954. Nota Geognostica preliminare.

A2A S.p.A. 1956. Relazione Geognostica.

A2A S.p.A. 1990. Diga Valgrosina—Indagini geofisiche con metodi sonici.

A2A S.p.A. 1990. Diga Valgrosina—Indagini sul calcestruzzo e roccia di fondazione.

A2A S.p.A. 1990. Diga Valgrosina—Prove di laboratorio su campioni di calcestruzzo e *roccia*.

A2A S.p.A. 2010. Pdg Valgrosina.

Addor, N., G. Nearing, C. Prieto, A. J. Newman, N. Le Vine, and M. P. Clark. 2018. "A Ranking of Hydrological Signatures Based on Their Predictability in Space." *Water Resources Research* 54, no. 11: 8792–8812. https://doi.org/10.1029/2018WR022606.

AghaKouchak, A., A. Bárdossy, and E. Habib. 2010. "Copula-Based Uncertainty Modelling: Application to Multisensor Precipitation Estimates." *Hydrological Processes* 24: 2111–2124. https://doi.org/10.1002/hyp.7632.

Akaike, H. 1974. "A New Look at the Statistical Model Identification." *IEEE Transactions on Automatic Control* 19, no. 6: 716–723. https://doi.org/10.1109/TAC.1974.1100705.

Alidoost, F., A. Stein, Z. Su, and A. Sharifi. 2017. "Three Novel Copula-Based bias Correction Methods for Daily ECMWF Air Temperature Data." *Hydrology and Earth System Sciences Discussions*. https://doi.org/10.5194/hess-2017-93.

Anagnostou, M. N., J. Kalogiros, E. N. Anagnostou, M. Tarolli, A. Papadopoulos, and M. Borga. 2010. "Performance Evaluation of High-Resolution Rainfall Estimation by X-Band Dual-Polarization Radar for Flash Flood Applications in Mountainous Basins." *Journal of Hydrology* 394, no. 1–2: 4–16. https://doi.org/10.1016/j.jhydrol.2010.06.026.

Andersson, J. C. M., B. Arheimer, F. Traoré, D. Gustafsson, and A. Ali. 2017. "Process Refinements Improve a Hydrological Model Concept Applied to The Niger River Basin." *Hydrological Processes* 31, no. 25: 4540–4554. https://doi.org/10.1002/hyp.11376.

Arnone, E., V. Zoratti, G. Formetta, S. Bosa, and M. Petti. 2023. "Predicting Peakflows in Mountain River Basins and Data-Scarce Areas: A Case Study in Northeastern Italy." *Hydrological Sciences Journal* 68, no. 3: 432–447. https://doi.org/10.1080/02626667.2022.2162408.

Asong, Z. E., M. E. Elshamy, D. Princz, et al. 2020. "High-Resolution Meteorological Forcing Data for Hydrological Modelling and Climate Change Impact Analysis in the Mackenzie River Basin." *Earth System Science Data* 12, no. 1: 629–645. https://doi.org/10.5194/essd-12-629-2020.

Assi, I., M. Barcella, G. B. Bischetti, R. Comolli, L. Folladori, and F. Previtali. 1995. "Suoli e ambiente della Val Grosina (Sondrio)." *Natura Bresciana* 31: 29–68.

Atlas, D. 1964. "Advances in Radar Meteorology." *Advances in Geophysics* 10: 317–478. https://doi.org/10.1016/S0065-2687(08)60009-6.

Bancheri, M. 2017. *A Flexible Approach to the Estimation of Water Budgets and Its Connection to the Travel Time Theory*. Trento, Italy: University of Trento.

Bancheri, M., R. Rigon, and S. Manfreda. 2020. "The GEOframe-NewAge Modelling System Applied in a Data Scarce Environment." *Watermark* 12, no. 1: 86. https://doi.org/10.3390/w12010086.

Bancheri, M., F. Serafin, M. Bottazzi, W. Abera, G. Formetta, and R. Rigon. 2018. "The Design, Deployment, and Testing of Kriging Models in GEOframe With SIK-0.9.8." *Geoscientific Model Development* 11, no. 6: 2189–2207. https://doi.org/10.5194/gmd-11-2189-2018.

Bancheri, M., F. Serafin, and R. Rigon. 2019. "The Representation of Hydrological Dynamical Systems Using Extended Petri Nets (EPN)." *Water Resources Research* 55, no. 11: 8895–8921. https://doi.org/10.1029/2019WR025099.

Bárdossy, A. 2006. "Copula-Based Geostatistical Models for Groundwater Quality Parameters." *Water Resources Research* 42, no. 11: W11416. https://doi.org/10.1029/2005WR004754.

Bárdossy, A., and J. Li. 2008. "Geostatistical Interpolation Using Copulas." *Water Resources Research* 44, no. 7: 15. https://doi.org/10.1029/2007WR006115.

Bárdossy, A., and G. Pegram. 2017. "Combination of Radar and Daily Precipitation Data to Estimate Meaningful Sub-Daily Point Precipitation Extremes." *Journal of Hydrology* 544: 397–406. https://doi.org/10.1016/j.jhydrol.2016.11.039.

Bell, V. A., and R. J. Moore. 2000. "The Sensitivity of Catchment Runoff Models to Rainfall Data at Different Spatial Scales." *Hydrology and Earth System Sciences* 4, no. 4: 653–667. https://doi.org/10.5194/hess-4-653-2000.

Belloni, S., and M. Pelfini. 1987. "Il gradiente termico in Lombardia." *Acqua-Aria* 4: 441–447.

Beltrami, G., C. Bianchi, G. Bonsignore, et al. 1971. "Carta geologica d'Italia alla scala 1:100.000: Foglio Tirano e note illustrative." *Ministry of Industry and Commerce*: 124.

Berndt, C., E. Rabiei, and U. Haberlandt. 2014. "Geostatistical Merging of Rain Gauge and Radar Data for High Temporal Resolutions and Various Station Density Scenarios." *Journal of Hydrology* 508: 88–101. https://doi.org/10.1016/j.jhydrol.2013.10.028.

Berne, A., and W. F. Krajewski. 2013. "Radar for Hydrology: Unfulfilled Promise or Unrecognized Potential?" *Advances in Water Resources* 51: 357–366. https://doi.org/10.1016/j.advwatres.2012.05.005.

Biggs, E. M., and P. M. Atkinson. 2011. "A Comparison of Gauge and Radar Precipitation Data for Simulating an Extreme Hydrological Event in the Severn Uplands, UK." *Hydrological Processes* 25, no. 5: 795–810. https://doi.org/10.1002/hyp.7869.

Bocchiola, D., and R. Rosso. 2014. "Safety of Italian Dams in the Face of Flood Hazard." *Advances in Water Resources* 71: 23–31. https://doi.org/10.1016/j.advwatres.2014.05.006.

Bonsignore, G., G. C. Bortolami, G. Elter, et al. 1969. "Carta Geologica di Italia 1:100000, Foglio 56. Note Illustrative."

Borga, M., F. Tonelli, R. J. Moore, and H. Andrieu. 2002. "Long-Term Assessment of bias Adjustment in Radar Rainfall Estimation." *Water Resources Research* 38, no. 11: 10. https://doi.org/10.1029/2001WR000555.

Braca, G., S. Mariani, B. Lastoria, et al. 2023. *Bilancio idrologico nazionale: Focus su siccità e disponibilità naturale della risorsa idrica rinnovabile*. Rome, Italy: ISPRA.

Buytaert, W., R. Celleri, P. Willems, B. D. Bièvre, and G. Wyseure. 2006. "Spatial and Temporal Rainfall Variability in Mountainous Areas: A Case Study From the South Ecuadorian Andes." *Journal of Hydrology* 329, no. 3–4: 413–421. https://doi.org/10.1016/j.jhydrol.2006.02.031.

Camera, C., A. Bruggeman, P. Hadjinicolaou, S. Pashiardis, and M. A. Lange. 2014. "Evaluation of Interpolation Techniques for the Creation of Gridded Daily Precipitation (1×1 km^2); Cyprus, 1980–2010." *Journal of Geophysical Research: Atmospheres* 119, no. 2: 693–712. https://doi.org/10.1002/2013JD020611.

Caruso, C., and F. Quarta. 1998. "Interpolation Methods Comparison." *Computers & Mathematics with Applications* 35, no. 12: 109–126. https://doi.org/10.1016/S0898-1221(98)00101-1.

Cecinati, F., O. Wani, and M. A. Rico-Ramirez. 2017. "Comparing Approaches to Deal With Non-Gaussianity of Rainfall Data in Kriging-Based Radar-Gauge Rainfall Merging." *Water Resources Research* 53, no. 11: 8999–9018. https://doi.org/10.1002/2016WR020330.

Chai, T., and R. R. Draxler. 2014. "Root Mean Square Error (RMSE) or Mean Absolute Error (MAE)? – Arguments Against Avoiding RMSE in the Literature." *Geoscientific Model Development* 7, no. 3: 1247–1250. https://doi.org/10.5194/gmd-7-1247-2014.

Charlton, R., R. Fealy, S. Moore, J. Sweeney, and C. Murphy. 2006. "Assessing the Impact of Climate Change on Water Supply and Flood Hazard in Ireland Using Statistical Downscaling and Hydrological Modelling Techniques." *Climatic Change* 74, no. 4: 475–491. https://doi.org/10.1007/s10584-006-0472-x.

Cheng, M., Y. Wang, B. Engel, et al. 2017. "Performance Assessment of Spatial Interpolation of Precipitation for Hydrological Process Simulation in the Three Gorges Basin." *Watermark* 9, no. 11: 838. https://doi.org/10.3390/w9110838.

Cochand, F., R. Therrien, and J.-M. Lemieux. 2019. "Integrated Hydrological Modeling of Climate Change Impacts in a Snow-Influenced Catchment: F. Cochand Et al. Groundwater XX, No. XX: XX-XX." *Groundwater* 57, no. 1: 3–20. https://doi.org/10.1111/gwat.12848.

Cornelissen, T., B. Diekkrüger, and S. Giertz. 2013. "A Comparison of Hydrological Models for Assessing the Impact of Land Use and Climate Change on Discharge in a Tropical Catchment." *Journal of Hydrology* 498: 221–236. https://doi.org/10.1016/j.jhydrol.2013.06.016.

Dai, Q., D. Han, M. A. Rico-Ramirez, and T. Islam. 2014. "Modelling Radar-Rainfall Estimation Uncertainties Using Elliptical and Archimedean Copulas With Different Marginal Distributions." *Hydrological Sciences Journal* 59, no. 11: 1992–2008. https://doi.org/10.1080/02626667.2013.865841.

Dai, Q., D. Han, L. Zhuo, J. Zhang, T. Islam, and P. K. Srivastava. 2016. "Seasonal Ensemble Generator for Radar Rainfall Using Copula and Autoregressive Model." *Stochastic Environmental Research and Risk Assessment* 30, no. 1: 27–38. https://doi.org/10.1007/s00477-014-1017-x.

Decloedt, L. C., P. Willems, and A. Gires. 2013. *Review Document: Methods and Experiences in Radar Based Fine Scale Rainfall Estimation*. Leuven, Belgium: Interreg RainGain Project.

Delaunay, B. 1934. "Sur la sphere vide." *Izv. Akad. Nauk SSSR, Otdelenie Matematicheskii i Estestvennyka Nauk* 7, no. 793–800: 1–2.

Delrieu, G., A. Wijbrans, B. Boudevillain, D. Faure, L. Bonnifait, and P.-E. Kirstetter. 2014. "Geostatistical Radar–Raingauge Merging: A Novel Method for the Quantification of Rain Estimation Accuracy." *Advances in Water Resources* 71: 110–124. https://doi.org/10.1016/j.advwatres.2014.06.005.

Devia, G. K., B. P. Ganasri, and G. S. Dwarakish. 2015. "A Review on Hydrological Models." *Aquatic Procedia* 4: 1001–1007. https://doi.org/10.1016/j.aqpro.2015.02.126.

Duan, Q. Y., V. K. Gupta, and S. Sorooshian. 1993. "Shuffled Complex Evolution Approach for Effective and Efficient Global Minimization." *Journal of Optimization Theory and Applications* 76, no. 3: 501–521. https://doi.org/10.1007/BF00939380.

Duchon, J. 1977. "Splines Minimizing Rotation-Invariant Semi-Norms in Sobolev Spaces." In *Constructive Theory of Functions of Several Variables*, edited by I. W. Schempp and K. Zeller, vol. 571, 85–100. Berlin Heidelberg: Springer. https://doi.org/10.1007/BFb0086566.

Ehret, U. 2002. *Rainfall and Flood Nowcasting in Small Catchments Using Weather Radar*. Stuttgart, Germany: University of Stuttgart.

Foehn, A., J. García Hernández, B. Schaefli, and G. De Cesare. 2018. "Spatial Interpolation of Precipitation From Multiple Rain Gauge Networks and Weather Radar Data for Operational Applications in Alpine Catchments." *Journal of Hydrology* 563: 1092–1110. https://doi.org/10.1016/j.jhydrol.2018.05.027.

Forcella, F. 1984. "Brevi note sulla tettonica gravitativa di versante nelle Alpi Centrali." *Bollettino della Societa Geologica Italiana* 103, no. 4: 689–696.

Formetta, G., A. Antonello, S. Franceschi, O. David, and R. Rigon. 2014. "Hydrological Modelling With Components: A GIS-Based Open-Source Framework." *Environmental Modelling & Software* 55: 190–200. https://doi.org/10.1016/j.envsoft.2014.01.019.

Fossati, D., and G. Mannucci. 1996. "L'alluvione del 1987 in Valtellina e l'evento franoso della Val Pola." *Documenti del Territorio (Centro Interregionale)* 14, no. 89: 37–44.

Gao, J., and D. J. Stensrud. 2012. "Assimilation of Reflectivity Data in a Convective-Scale, Cycled 3DVAR Framework With Hydrometeor Classification." *Journal of the Atmospheric Sciences* 69, no. 3: 1054–1065. https://doi.org/10.1175/JAS-D-11-0162.1.

Germann, U., G. Galli, M. Boscacci, and M. Bolliger. 2006. "Radar Precipitation Measurement in a Mountainous Region." *Quarterly Journal of the Royal Meteorological Society* 132, no. 618: 1669–1692. https://doi.org/10.1256/qj.05.190.

Gilewski, P. 2021. "Impact of the Grid Resolution and Deterministic Interpolation of Precipitation on Rainfall-Runoff Modeling in a Sparsely Gauged Mountainous Catchment." *Watermark* 13, no. 2: 230. https://doi.org/10.3390/w13020230.

Gómez-Hernández, J. J., and X.-H. Wen. 1998. "To Be or Not to Be Multi-Gaussian? A Reflection on Stochastic Hydrogeology." *Advances in Water Resources* 21, no. 1: 47–61. https://doi.org/10.1016/S0309-1708(96)00031-0.

Gorgucci, E., and V. Chandrasekar. 2005. "Evaluation of Attenuation Correction Methodology for Dual-Polarization Radars: Application to X-Band Systems." *Journal of Atmospheric and Oceanic Technology* 22, no. 8: 1195–1206. https://doi.org/10.1175/JTECH1763.1.

Gräler, B., E. J. Pebesma, and G. B. Heuvelink. 2016. "Spatio-Temporal Interpolation using gstat." *Spatio-Temporal Interpolation Using Gstat. R J* 8, no. 1: 204.

Gregnanin, A., and A. Montrasio. 1990. "Struttura ed evoluzione delle Unità Sudalpine. Il basamento." In *Guide Geologiche Regionali - Alpi e Prealpi Lombarde*, 24–25. Bologna, Italy: BE-MA Editrice.

Groisman, P. Y., and D. R. Easterling. 1994. "Variability and Trends of Total Precipitation and Snowfall Over the United States and Canada." *Journal of Climate* 7, no. 1: 184–205. https://doi.org/10.1175/1520-0442(1994)007<0184:VATOTP>2.0.CO;2.

Gupta, H. V., H. Kling, K. K. Yilmaz, and G. F. Martinez. 2009. "Decomposition of the Mean Squared Error and NSE Performance Criteria: Implications for Improving Hydrological Modelling." *Journal of Hydrology* 377, no. 1–2: 80–91. https://doi.org/10.1016/j.jhydrol.2009.08.003.

Haberlandt, U. 2007. "Geostatistical Interpolation of Hourly Precipitation From Rain Gauges and Radar for a Large-Scale Extreme Rainfall Event." *Journal of Hydrology* 332, no. 1–2: 144–157. https://doi.org/10.1016/j.jhydrol.2006.06.028.

Hamidi, A., D. J. Farnham, and R. Khanbilvardi. 2018. "Uncertainty Analysis of Urban Sewer System Using Spatial Simulation of Radar Rainfall Fields: New York City Case Study." *Stochastic Environmental Research and Risk Assessment* 32, no. 8: 2293–2308. https://doi.org/10.1007/s00477-018-1563-8.

Hegerl, G. C., E. Black, R. P. Allan, et al. 2015. "Challenges in Quantifying Changes in the Global Water Cycle." *Bulletin of the American Meteorological Society* 96, no. 7: 1097–1115. https://doi.org/10.1175/BAMS-D-13-00212.1.

Hock, R. 1999. "A Distributed Temperature-Index Ice- and Snowmelt Model Including Potential Direct Solar Radiation." *Journal of Glaciology* 45, no. 149: 101–111. https://doi.org/10.3189/S0022143000003087.

Idso, S. B. 1981. "A Set of Equations for Full Spectrum and 8- To 14-μm and 10.5- To 12.5-μm Thermal Radiation From Cloudless Skies." *Water*

Resources Research 17, no. 2: 295–304. https://doi.org/10.1029/WR017i002p00295.

Johnson, G. L., and C. L. Hanson. 1995. "Topographic and Atmospheric Influences on Precipitation Variability Over a Mountainous Watershed." *Journal of Applied Meteorology* 34, no. 1: 68–87. https://doi.org/10.1175/1520-0450-34.1.68.

Jordan, Y. C., A. Ghulam, and S. Hartling. 2014. "Traits of Surface Water Pollution Under Climate and Land Use Changes: A Remote Sensing and Hydrological Modeling Approach." *Earth-Science Reviews* 128: 181–195. https://doi.org/10.1016/j.earscirev.2013.11.005.

Karlsson, I. B., T. O. Sonnenborg, J. C. Refsgaard, et al. 2016. "Combined Effects of Climate Models, Hydrological Model Structures and Land Use Scenarios on Hydrological Impacts of Climate Change." *Journal of Hydrology* 535: 301–317. https://doi.org/10.1016/j.jhydrol.2016.01.069.

Kim, T.-J., H.-H. Kwon, and C. Lima. 2018. "A Bayesian Partial Pooling Approach to Mean Field bias Correction of Weather Radar Rainfall Estimates: Application to Osungsan Weather Radar in South Korea." *Journal of Hydrology* 565: 14–26. https://doi.org/10.1016/j.jhydrol.2018.07.082.

Kling, H., M. Fuchs, and M. Paulin. 2012. "Runoff Conditions in the Upper Danube Basin Under an Ensemble of Climate Change Scenarios." *Journal of Hydrology* 424–425: 264–277. https://doi.org/10.1016/j.jhydrol.2012.01.011.

Krause, P., D. P. Boyle, and F. Bäse. 2005. "Comparison of Different Efficiency Criteria for Hydrological Model Assessment." *Advances in Geosciences* 5: 89–97. https://doi.org/10.5194/adgeo-5-89-2005.

Ladson, A., R. Brown, B. Neal, and R. Nathan. 2013. "A Standard Approach to Baseflow Separation Using the Lyne and Hollick Filter." *Australian Journal of Water Resources* 17, no. 1: 25–34. https://doi.org/10.7158/W12-028.2013.17.1.

Lazoglou, G., B. Gräler, and C. Anagnostopoulou. 2019. "Simulation of Extreme Temperatures Using a New Method: TIN-Copula." *International Journal of Climatology* 39, no. 13: 5201–5214. https://doi.org/10.1002/joc.6124.

Lazoglou, G., G. Zittis, C. Anagnostopoulou, P. Hadjinicolaou, and J. Lelieveld. 2020. "Bias Correction of RCM Precipitation by TIN-Copula Method: A Case Study for Historical and Future Simulations in Cyprus." *Climate* 8, no. 7: 85. https://doi.org/10.3390/cli8070085.

Lazoglou, G., G. Zittis, P. Hadjinicolaou, and J. Lelieveld. 2022. "TIN-Copula bias-Correction Method for Model-Derived Maximum Temperature in the MENA Region." *International Journal of Climatology* 42, no. 4: 2260–2280. https://doi.org/10.1002/joc.7364.

Ly, S., C. Charles, and A. Degré. 2013. "Different Methods for Spatial Interpolation of Rainfall Data for Operational Hydrology and Hydrological Modeling at Watershed Scale. A Review." *Biotechnologie, Agronomie, Société et Environnement* 17, no. 2: 392–406.

Madrazo-Uribeetxebarria, E., M. Garmendia Antín, J. Almandoz Berrondo, and I. Andrés-Doménech. 2021. "Sensitivity Analysis of Permeable Pavement Hydrological Modelling in the Storm Water Management Model." *Journal of Hydrology* 600: 126525. https://doi.org/10.1016/j.jhydrol.2021.126525.

Mair, A., and A. Fares. 2011. "Comparison of Rainfall Interpolation Methods in a Mountainous Region of a Tropical Island." *Journal of Hydrologic Engineering* 16, no. 4: 371–383. https://doi.org/10.1061/(ASCE)HE.1943-5584.0000330.

Maity, R., M. Suman, P. Laux, and H. Kunstmann. 2019. "Bias Correction of Zero-Inflated RCM Precipitation Fields: A Copula-Based Scheme for Both Mean and Extreme Conditions." *Journal of Hydrometeorology* 20, no. 4: 595–611. https://doi.org/10.1175/JHM-D-18-0126.1.

Mao, G., S. Vogl, P. Laux, S. Wagner, and H. Kunstmann. 2015. "Stochastic bias Correction of Dynamically Downscaled Precipitation Fields for Germany Through Copula-Based Integration of Gridded Observation Data." *Hydrology and Earth System Sciences* 19, no. 4: 1787–1806. https://doi.org/10.5194/hess-19-1787-2015.

Mapiam, P. P., M. Methaprayun, T. Bogaard, G. Schoups, and M.-C. Ten Veldhuis. 2022. "Citizen Rain Gauges Improve Hourly Radar Rainfall bias Correction Using a Two-Step Kalman Filter." *Hydrology and Earth System Sciences* 26, no. 3: 775–794. https://doi.org/10.5194/hess-26-775-2022.

McCully, P. 2001. *Silenced Rivers: The Ecology and Politics of Large Dams*. New York, NY: Enlarged & updated edition Zed Books.

Mudashiru, R. B., N. Sabtu, I. Abustan, and W. Balogun. 2021. "Flood Hazard Mapping Methods: A Review." *Journal of Hydrology* 603: 126846. https://doi.org/10.1016/j.jhydrol.2021.126846.

Nash, J. E., and J. V. Sutcliffe. 1970. "River Flow Forecasting Through Conceptual Models Part I—A Discussion of Principles." *Journal of Hydrology* 10, no. 3: 282–290. https://doi.org/10.1016/0022-1694(70)90255-6.

Norman, L. M., H. Huth, L. Levick, et al. 2010. "Flood Hazard Awareness and Hydrologic Modelling at Ambos Nogales, United States–Mexico Border." *Journal of Flood Risk Management* 3, no. 2: 151–165. https://doi.org/10.1111/j.1753-318X.2010.01066.x.

Notarpietro, A. 1988. *Appunti e considerazioni sulla geologia dell'alta Valtellina*. Milan, Italy: Centro di Studio per la Stratigrafia e Petrografia delle Alpi Centrali del C.N.R.

Nychka, D., R. Furrer, J. Paige, and S. Sain. 2017. "Fields: Tools for Spatial Data." R Package Versions 10:3. https://doi.org/10.5065/D6W957CT.

Ochoa-Rodriguez, S., L.-P. Wang, P. Willems, and C. Onof. 2019. "A Review of Radar-Rain Gauge Data Merging Methods and Their Potential for Urban Hydrological Applications." *Water Resources Research* 55, no. 8: 6356–6391. https://doi.org/10.1029/2018WR023332.

Paul, M., A. Rajib, M. Negahban-Azar, A. Shirmohammadi, and P. Srivastava. 2021. "Improved Agricultural Water Management in Data-Scarce Semi-Arid Watersheds: Value of Integrating Remotely Sensed Leaf Area Index in Hydrological Modeling." *Science of the Total Environment* 791: 148177. https://doi.org/10.1016/j.scitotenv.2021.148177.

Pebesma, E. J. 2004. "Multivariable Geostatistics in S: The Gstat Package." *Computers & Geosciences* 30, no. 7: 683–691. https://doi.org/10.1016/j.cageo.2004.03.012.

Peirce, C. S. 1884. "The Numerical Measure of the Success of Predictions." *Science* 93: 453–454. https://doi.org/10.1126/science.ns-4.93.453-a.

Pozzi, R., G. Bollettinari, and A. Clerici. 1990. *Studio geomorfologico e geologico applicato dell'Alta Valtellina: Alto bacino dell'Adda con chiusura a Tirano*, 151. Milan, Italy: AEM: Azienda Energetica Municipale.

Priestley, C. H. B., and R. J. Taylor. 1972. "On the Assessment of Surface Heat Flux and Evaporation Using Large-Scale Parameters." *Monthly Weather Review* 100, no. 2: 81–92. https://doi.org/10.1175/1520-0493(1972)100<0081:OTAOSH>2.3.CO;2.

Qin, H., G. Cao, M. Kristensen, et al. 2013. "Integrated Hydrological Modeling of the North China Plain and Implications for Sustainable Water Management." *Hydrology and Earth System Sciences* 17, no. 10: 3759–3778. https://doi.org/10.5194/hess-17-3759-2013.

Rabiei, E., and U. Haberlandt. 2015. "Applying bias Correction for Merging Rain Gauge and Radar Data." *Journal of Hydrology* 522: 544–557. https://doi.org/10.1016/j.jhydrol.2015.01.020.

Reichle, R. H., and R. D. Koster. 2004. "Bias Reduction in Short Records of Satellite Soil Moisture." *Geophysical Research Letters* 31, no. 19: 19501. https://doi.org/10.1029/2004GL020938.

Renka, R. J., A. Gebhardt, S. Eglen, S. Zuyev, and D. White. 2020. "Tripack: Triangulation of Irregularly Spaced Data (Versione 1.3–9) [Software]."

Rogers, R. R., and P. L. Smith. 1996. "A Short History of Radar Meteorology." In *Historical Essays on Meteorology 1919–1995*, edited by J. R. Fleming, 57–98. Boston, MA: American Meteorological Society. https://doi.org/10.1007/978-1-940033-84-6_4.

Sampson, C. C., A. M. Smith, P. D. Bates, J. C. Neal, L. Alfieri, and J. E. Freer. 2015. "A High-Resolution Global Flood Hazard Model: A High-Resolution Global Flood Hazard Model." *Water Resources Research* 51, no. 9: 7358–7381. https://doi.org/10.1002/2015WR016954.

Segond, M.-L., H. S. Wheater, and C. Onof. 2007. "The Significance of Spatial Rainfall Representation for Flood Runoff Estimation: A Numerical Evaluation Based on the Lee Catchment, UK." *Journal of Hydrology* 347, no. 1–2: 116–131. https://doi.org/10.1016/j.jhydrol.2007.09.040.

Seo, D.-J. 1998. "Real-Time Estimation of Rainfall Fields Using Radar Rainfall and Rain Gage Data." *Journal of Hydrology* 208, no. 1–2: 37–52. https://doi.org/10.1016/S0022-1694(98)00141-3.

Seo, D.-J., and J. P. Breidenbach. 2002. "Real-Time Correction of Spatially Nonuniform Bias in Radar Rainfall Data Using Rain Gauge Measurements." *Journal of Hydrometeorology* 3, no. 2: 93–111. https://doi.org/10.1175/1525-7541(2002)003<0093:RTCOSN>2.0.CO;2.

Seo, D.-J., J. P. Breidenbach, and E. R. Johnson. 1999. "Real-Time Estimation of Mean Field bias in Radar Rainfall Data." *Journal of Hydrology* 223, no. 3–4: 131–147. https://doi.org/10.1016/S0022-1694(99)00106-7.

Sevruk, B. 1997. "Regional Dependency of Precipitation-Altitude Relationship in the Swiss Alps." In *Climatic Change at High Elevation Sites*, edited by H. F. In, M. B. Diaz, and R. S. Bradley, 123–137. Netherlands: Springer. https://doi.org/10.1007/978-94-015-8905-5_7.

Shakti, P. C., M. Maki, S. Shimizu, et al. 2013. "Correction of Reflectivity in the Presence of Partial Beam Blockage Over a Mountainous Region Using X-Band Dual Polarization Radar." *Journal of Hydrometeorology* 14, no. 3: 744–764. https://doi.org/10.1175/JHM-D-12-077.1.

Shehu, B., and U. Haberlandt. 2021. "Relevance of Merging Radar and Rainfall Gauge Data for Rainfall Nowcasting in Urban Hydrology." *Journal of Hydrology* 594: 125931. https://doi.org/10.1016/j.jhydrol.2020.125931.

Shepard, D. 1968. "A Two-Dimensional Interpolation Function for Irregularly-Spaced Data." *Proceedings of the 1968 23rd ACM National Conference* 23: 517–524. https://doi.org/10.1145/800186.810616.

Sideris, I. V., M. Gabella, R. Erdin, and U. Germann. 2014. "Real-Time Radar-Rain-Gauge Merging Using Spatio-Temporal Co-Kriging With External Drift in the Alpine Terrain of Switzerland: Real-Time Radar-Rain-Gauge Merging." *Quarterly Journal of the Royal Meteorological Society* 140, no. 680: 1097–1111. https://doi.org/10.1002/qj.2188.

Sideris, I. V., M. Gabella, M. Sassi, and U. Germann. 2014. *Proceedings of the 2014 International Weather Radar and Hydrology Symposium*, 1–10.

Sinclair, S., and G. Pegram. 2005. "Combining Radar and Rain Gauge Rainfall Estimates Using Conditional Merging." *Atmospheric Science Letters* 6, no. 1: 19–22. https://doi.org/10.1002/asl.85.

Sinclair, M. R., D. S. Wratt, R. D. Henderson, and W. R. Gray. 1997. "Factors Affecting the Distribution and Spillover of Precipitation in the Southern Alps of New Zealand—A Case Study." *Journal of Applied Meteorology* 36, no. 5: 428–442. https://doi.org/10.1175/1520-0450(1997)036<0428:FATDAS>2.0.CO;2.

Singh, A. 2022. "CDF Matching bias Correction Method in MATLAB." MATLAB Central File Exchange. https://www.mathworks.com/matlabcentral/fileexchange/78784-cdf-matching-bias-correction-method-in-matlab.

Sklar, M. 1959. "Fonctions de repartition an dimensions et leurs marges." *Publications de l'Institut de statistique de l'Université de Paris* 8: 229–231.

Snyder, J. C., H. B. Bluestein, G. Zhang, and S. J. Frasier. 2010. "Attenuation Correction and Hydrometeor Classification of High-Resolution, X-Band, Dual-Polarized Mobile Radar Measurements in Severe Convective Storms." *Journal of Atmospheric and Oceanic Technology* 27, no. 12: 1979–2001. https://doi.org/10.1175/2010JTECHA1356.1.

Sofokleous, I., A. Bruggeman, S. Michaelides, P. Hadjinicolaou, G. Zittis, and C. Camera. 2021. "Comprehensive Methodology for the Evaluation of High-Resolution WRF Multiphysics Precipitation Simulations for Small, Topographically Complex Domains." *Journal of Hydrometeorology* 22, no. 5: 1169–1186. https://doi.org/10.1175/JHM-D-20-0110.1.

Sokol, Z., J. Szturc, J. Orellana-Alvear, J. Popová, A. Jurczyk, and R. Célleri. 2021. "The Role of Weather Radar in Rainfall Estimation and Its Application in Meteorological and Hydrological Modelling—A Review." *Remote Sensing* 13, no. 3: 351. https://doi.org/10.3390/rs13030351.

Stockham, A. J., D. M. Schultz, J. G. Fairman, and A. P. Draude. 2018. "Quantifying the Rain-Shadow Effect: Results From the Peak District, British Isles." *Bulletin of the American Meteorological Society* 99, no. 4: 777–790. https://doi.org/10.1175/BAMS-D-17-0256.1.

Teegavarapu, R. S. V., T. Meskele, and C. S. Pathak. 2012. "Geo-Spatial Grid-Based Transformations of Precipitation Estimates Using Spatial Interpolation Methods." *Computers & Geosciences* 40: 28–39. https://doi.org/10.1016/j.cageo.2011.07.004.

Terna. 2022. Dati statistici sull'energia elettrica in Italia.

Thorndahl, S., T. Einfalt, P. Willems, et al. 2017. "Weather Radar Rainfall Data in Urban Hydrology." *Hydrology and Earth System Sciences* 21, no. 3: 1359–1380. https://doi.org/10.5194/hess-21-1359-2017.

Toso, F. C. 2014. "A Hydroelectric Landscape in the Italian Alps: Elements, Meanings, and Design Cues in a Historical Hydroelectric Development in Alta Valtellina." *Journal of Landscape Architecture* 9, no. 2: 30–39. https://doi.org/10.1080/18626033.2014.931700.

Towner, J., H. L. Cloke, E. Zsoter, et al. 2019. "Assessing the Performance of Global Hydrological Models for Capturing Peak River Flows in the Amazon Basin." *Hydrology and Earth System Sciences* 23, no. 7: 3057–3080. https://doi.org/10.5194/hess-23-3057-2019.

University of Bern - Institute of Geology, & Federal Office for Water and Geology. 2005. "Geologische Karte der Schweiz 1:500 000."

Van Den Hende, C., B. Van Schaeybroeck, J. Nyssen, S. Van Vooren, M. Van Ginderachter, and P. Termonia. 2021. "Analysis of Rain-Shadows in the Ethiopian Mountains Using Climatological Model Data." *Climate Dynamics* 56, no. 5–6: 1663–1679. https://doi.org/10.1007/s00382-020-05554-2.

Velasco-Forero, C. A., D. Sempere-Torres, E. F. Cassiraga, and J. Jaime Gómez-Hernández. 2009. "A Non-parametric Automatic Blending Methodology to Estimate Rainfall Fields From Rain Gauge and Radar Data." *Advances in Water Resources* 32, no. 7: 986–1002. https://doi.org/10.1016/j.advwatres.2008.10.004.

Villarini, G., B.-C. Seo, F. Serinaldi, and W. F. Krajewski. 2014. "Spatial and Temporal Modeling of Radar Rainfall Uncertainties." *Atmospheric Research* 135–136: 91–101. https://doi.org/10.1016/j.atmosres.2013.09.007.

Vogl, S., P. Laux, W. Qiu, G. Mao, and H. Kunstmann. 2012. "Copula-Based Assimilation of Radar and Gauge Information to Derive bias-Corrected Precipitation Fields." *Hydrology and Earth System Sciences* 16, no. 7: 2311–2328. https://doi.org/10.5194/hess-16-2311-2012.

Wang, L.-P., S. Ochoa-Rodríguez, N. E. Simões, C. Onof, and Č. Maksimović. 2013. "Radar–Raingauge Data Combination Techniques: A Revision and Analysis of Their Suitability for Urban Hydrology." *Water Science and Technology* 68, no. 4: 737–747. https://doi.org/10.2166/wst.2013.300.

Wegehenkel, M. 2002. "Estimating of the Impact of Land Use Changes Using the Conceptual Hydrological Model THESEUS—A Case Study."

Physics and Chemistry of the Earth, Parts A/B/C 27, no. 9–10: 631–640. https://doi.org/10.1016/S1474-7065(02)00047-5.

Weisse, A. K., and P. Bois. 2001. "Topographic Effects on Statistical Characteristics of Heavy Rainfall and Mapping in the French Alps." *Journal of Applied Meteorology* 40, no. 4: 720–740. https://doi.org/10.1175/1520-0450(2001)040<0720:TEOSCO>2.0.CO;2.

World Commission on Dams (A c. Di). 2000. *Dams and Development: A New Framework for Decision-Making*. London, UK: Earthscan Publications Ltd.

Wright, D. B., J. A. Smith, G. Villarini, and M. L. Baeck. 2014. "Long-Term High-Resolution Radar Rainfall Fields for Urban Hydrology." *JAWRA Journal of the American Water Resources Association* 50, no. 3: 713–734. https://doi.org/10.1111/jawr.12139.

Yan, B., N. F. Fang, P. C. Zhang, and Z. H. Shi. 2013. "Impacts of Land Use Change on Watershed Streamflow and Sediment Yield: An Assessment Using Hydrologic Modelling and Partial Least Squares Regression." *Journal of Hydrology* 484: 26–37. https://doi.org/10.1016/j.jhydrol.2013.01.008.

Yazdandoost, F., S. Moradian, M. Zakipour, A. Izadi, and M. Bavandpour. 2020. "Improving the Precipitation Forecasts of the North-American Multi Model Ensemble (NMME) Over Sistan Basin." *Journal of Hydrology* 590: 125263. https://doi.org/10.1016/j.jhydrol.2020.125263.

Zhang, H., B. Wang, D. L. Liu, M. Zhang, L. M. Leslie, and Q. Yu. 2020. "Using an Improved SWAT Model to Simulate Hydrological Responses to Land Use Change: A Case Study of a Catchment in Tropical Australia." *Journal of Hydrology* 585: 124822. https://doi.org/10.1016/j.jhydrol.2020.124822.

Appendix A

T – Temperature
P – Precipitation
P_r – Rainfall
P_s – Snow
SWE – Snow Water Equivalent
M – Melted water
W_s – Water liquid snow storage
R – Refreezing
M_d – Melting discharge
S_c – Canopy storage
ET_c – Canopy evapotranspiration
T_r – Throughfall
U_1 – Quick flow
U_2 – Slow flow
F – Partition Function
S_{RZ} – Root zone storage
ET_{RZ} – Root zone evapotranspiration
R_e – Groundwater recharge
S_{GW} – Groundwater storage
Q_{GW} – Groundwater flow
S_R – Runoff storage
Q_R – Runoff flow
Q_T – Simulated total streamflow

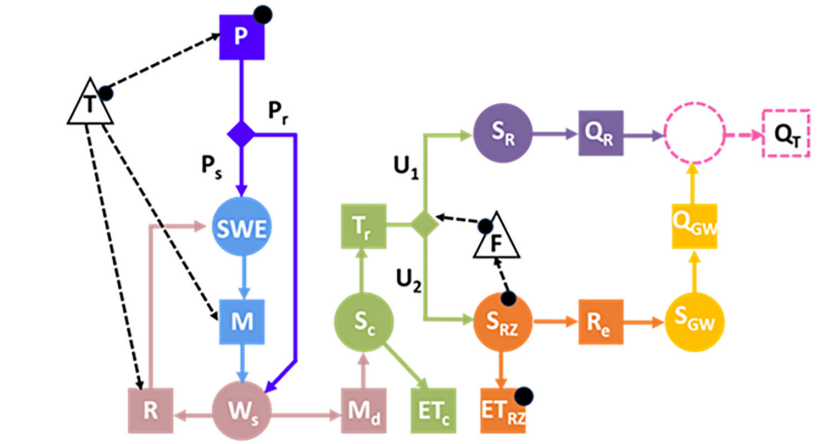

Precipitation | Snowmelt | Root zone | Surface waters
Snow | Canopy | Groundwater | Simulated discharge

FIGURE A1 | Schematic diagram of components and their connection in the GEOframe hydrological system using Petri Nets representation (Bancheri, Serafin, and Rigon 2019) (modified from GEOframe Winter school supporting material).

TABLE A1 | Weather stations representing the triangle vertexes used to carry out the LOO cross-validation test on a specific rain gauge (first column) are listed in the table.

Name	Station 1	Station 2	Station 3	k_a	k_b	k_c
A-Eita	Q-Valdisotto, Oga S.Colombano	N-Valdidentro, Arnoga	C-Grosio	0.29	0.33	0.38
B-Malghera	A-Eita	U-Poschiavo/Robbia	C-Grosio	0.27	0.42	0.31
C-Grosio	M-Tirano	J-Monno	A-Eita	0.26	0.29	0.46
D-Aprica	—	—	—	—	—	—
E-Bormio	R-Valfurva	O-Valdidentro, Cancano	P-Valdisotto, Arginone	0.23	0.41	0.37
F-Edolo, Ist. Meneghini	D-Aprica	G-Edolo, Pantano d'Avio	J-Monno	0.21	0.29	0.51
G-Edolo, Pantano d'Avio	—	——	—	—	—	—
H-Livigno, la Vallaccia	K-Livigno, Foscagno	S-Passo del Bernina	B-Malghera	0.76	0.11	0.14
K-Livigno, Foscagno	T-Buffalora	H-Livigno, la Vallaccia	O-Valdidentro, Cancano	0.11	0.72	0.17
J-Monno	F-Edolo, Ist. Meneghini	P-Valdisotto, Arginone	C-Grosio	0.43	0.24	0.34
I-Ponte di Legno	—	—	—	—	—	—
L-Teglio	—	—	—	—	—	—
M-Tirano	B-Malghera	D-Aprica	C-Grosio	0.35	0.31	0.33
N-Valdidentro, Arnoga	Q-Valdisotto, Oga S.Colombano	K-Livigno, Foscagno	A-Eita	0.31	0.41	0.28
O-Valdidentro, Cancano	E-Bormio	T-Buffalora	Q-Valdisotto, Oga S.Colombano	0.37	0.19	0.44
P-Valdisotto, Arginone	I-Ponte di Legno	E-Bormio	J-Monno	0.23	0.49	0.28
Q-Valdisotto, Oga S. Colombano	E-Bormio	N-Valdidentro, Arnoga	P-Valdisotto, Arginone	0.35	0.37	0.28
R-Valfurva	—	—	—	—	—	—
S-Passo del Bernina	—	—	—	—	—	—
T-Buffalora	—	—	—	—	—	—
U-Poschiavo/Robbia	S-Passo del Bernina	L-Teglio	B-Malghera	0.42	0.17	0.41
V-*S. Maria*	—	—	—	—	—	—

Note: The relative coefficients (function of the point-weather station distance) to perform the weighted average are also shown.

TABLE A2 | CSS and scaled scores SS (SS KGE, SS RMSE, SS EES and SS PSS) values for the Raw Radar data, Rain gauge TIN, Rain gauge OK, the point-based methods (TIN-copula, TIN-CDF bias correction), and spatial methods on residuals (Radar + IDW, Radar + TPS, Radar + OK and Radar + DK) considering the 14 stations in common are listed in the table.

	Raw Radar data	Rain gauge TIN	Rain gauge OK	TIN-copula	TIN-CDF	Radar + IDW	Radar + TPS	Radar + OK	Radar + DK
SS KGE	0.26	1.00	0.00	0.30	0.56	0.81	0.54	0.80	0.75
SS RMSE	0.37	0.00	0.55	0.18	0.35	0.67	0.48	1.00	0.62
CSS	0.33	0.68	0.22	0.28	0.35	0.71	0.66	0.87	0.75
SS EES	0.58	0.81	0.00	0.56	0.49	0.50	0.86	1.00	0.64
SS PSS	0.10	0.90	0.31	0.09	0.00	0.84	0.77	0.67	1.00

Note: The values range between 0 and 1 being scaled.

TABLE A3 | Weather stations representing the triangle vertexes used to correct the hourly radar precipitation series in the cell corresponding to the centroid sub-basin (first column) are listed in the table.

ID sub-basin	Station 1	Station 2	Station 3	k_{-a}	k_b	k_c
45	B-Malghera	M-Tirano	C-Grosio	0.35	0.36	0.29
39	B-Malghera	M-Tirano	C-Grosio	0.50	0.28	0.22
35	B-Malghera	M-Tirano	C-Grosio	0.25	0.26	0.49
34	B-Malghera	M-Tirano	C-Grosio	0.27	0.20	0.53
33	B-Malghera	M-Tirano	C-Grosio	0.34	0.22	0.44
32	B-Malghera	M-Tirano	C-Grosio	0.48	0.23	0.30
30	U-Poschiavo/Robbia	M-Tirano	B-Malghera	0.19	0.18	0.63
29	P-Valdisotto	A-Eita	C-Grosio	0.09	0.20	0.71
25	B-Malghera	U-Poschiavo/Robbia	M-Tirano	0.76	0.14	0.09
24	P-Valdisotto	A-Eita	C-Grosio	0.17	0.38	0.45
21	P-Valdisotto	A-Eita	C-Grosio	0.14	0.48	0.38
17	A-Eita	B-Malghera	C-Grosio	0.18	0.60	0.22
16	N-Valdidentro	B-Malghera	A-Eita	0.06	0.86	0.08
14	A-Eita	B-Malghera	C-Grosio	0.76	0.08	0.16
12	A-Eita	B-Malghera	C-Grosio	0.43	0.22	0.36
11	N-Valdidentro	B-Malghera	A-Eita	0.21	0.50	0.29
10	N-Valdidentro	B-Malghera	A-Eita	0.26	0.34	0.40
9	N-Valdidentro	S-Passo del Bernina	B-Malghera	0.15	0.14	0.71
8	P-Valdisotto	A-Eita	C-Grosio	0.26	0.50	0.24
6	Q-Valdisotto	A-Eita	P-Valdisotto	0.13	0.76	0.11
4	A-Eita	N-Valdidentro	B-Malghera	0.74	0.18	0.09

Note: The relative coefficients (function of the point-weather station distance) to perform the weighted average are also shown.

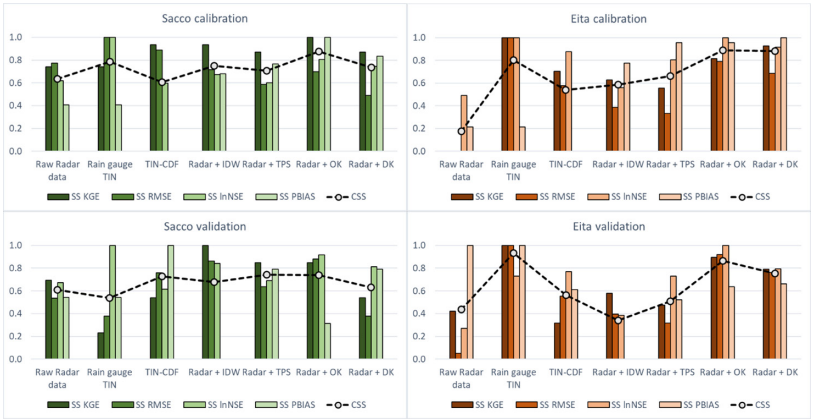

FIGURE A2 | Performance comparison using CSS values for the two basins and for both calibration and validation periods.

TABLE A4 | GEOframe parameters calibrated for the Sacco basin considering all the precipitation datasets.

Sacco basin	Raw radar data	Rain gauge TIN	TIN-CDF	Radar + IDW	Radar + TPS	Radar + OK	Radar + DK
α_r	0.93	0.91	1.11	0.83	0.92	0.88	0.82
α_s	1.19	0.97	1.18	0.59	0.56	0.80	0.83
Melting temperature	0.10	−0.18	0.32	−0.01	0.31	−0.49	−0.67
Combined Melting factor	0.88	0.93	0.79	0.97	0.94	0.97	0.74
α_l	0.70	0.82	0.76	0.77	0.88	0.65	0.73
Kc	0.59	0.45	0.70	0.57	0.78	0.31	0.46
p	0.85	0.86	0.80	0.89	0.63	0.76	0.11
s_RootZoneMax	38.40	34.74	43.16	149.13	97.81	94.56	70.83
g	7.99	7.36	2.54	5.23	0.55	2.46	1.44
h	1.10	2.31	1.36	2.49	2.84	2.57	2.62
pB_soil	1.11	2.79	0.49	1.58	1.55	2.20	2.01
s_RunoffMax	168.92	123.69	148.46	38.91	85.36	73.80	139.46
c	1.20	9.86	10.92	13.55	3.41	9.62	2.26
d	1.87	2.77	1.69	2.41	2.33	2.85	2.60
s_GroundWaterMax	193.90	181.93	114.35	164.75	122.67	190.17	82.11
e	6.65	1.84	5.21	7.82	9.92	3.52	8.63
f	2.19	2.48	2.20	1.95	1.97	1.36	1.41

TABLE A5 | GEOframe parameters calibrated for the Eita basin considering all the precipitation datasets.

Eita basin	Raw radar data	Rain gauge TIN	TIN-CDF	Radar + IDW	Radar + TPS	Radar + OK	Radar + DK
α_r	0.82	1.02	1.19	0.87	1.18	0.93	0.88
α_s	0.83	0.95	1.19	0.61	1.15	0.83	0.68
Melting temperature	−0.35	0.07	−0.19	0.20	−0.31	−0.27	−0.09
Combined Melting factor	0.90	0.87	0.76	0.97	0.54	0.98	0.99
α_l	0.60	0.81	0.78	0.80	0.71	0.61	0.83
Kc	0.59	0.21	0.28	0.53	0.18	0.36	0.68
p	0.74	0.81	0.70	0.83	0.90	0.67	0.68
s_RootZoneMax	96.65	109.78	65.26	135.74	79.94	107.78	49.25
g	0.95	3.69	6.41	6.33	8.87	1.37	1.73
h	2.85	2.37	2.44	2.55	1.01	2.59	2.33
pB_soil	1.73	1.79	1.86	0.99	1.37	1.48	2.18
s_RunoffMax	83.03	95.17	56.06	26.61	41.85	61.07	74.68
c	6.59	9.05	18.31	14.43	5.75	3.06	3.18
d	2.66	1.88	2.63	2.58	2.29	1.64	2.91
s_GroundWaterMax	78.02	105.84	283.12	158.79	107.09	239.00	233.56
e	5.98	2.57	5.69	6.85	1.90	9.13	7.13
f	1.93	2.99	1.22	1.52	1.91	2.05	1.71